

AD-A043 906

PHYSICS INTERNATIONAL CO SAN LEANDRO CALIF
IN SITU STRESS GAUGE CALIBRATION.(U)
MAY 77 K SEIFERT, J SHEA

F/G 19/4

UNCLASSIFIED

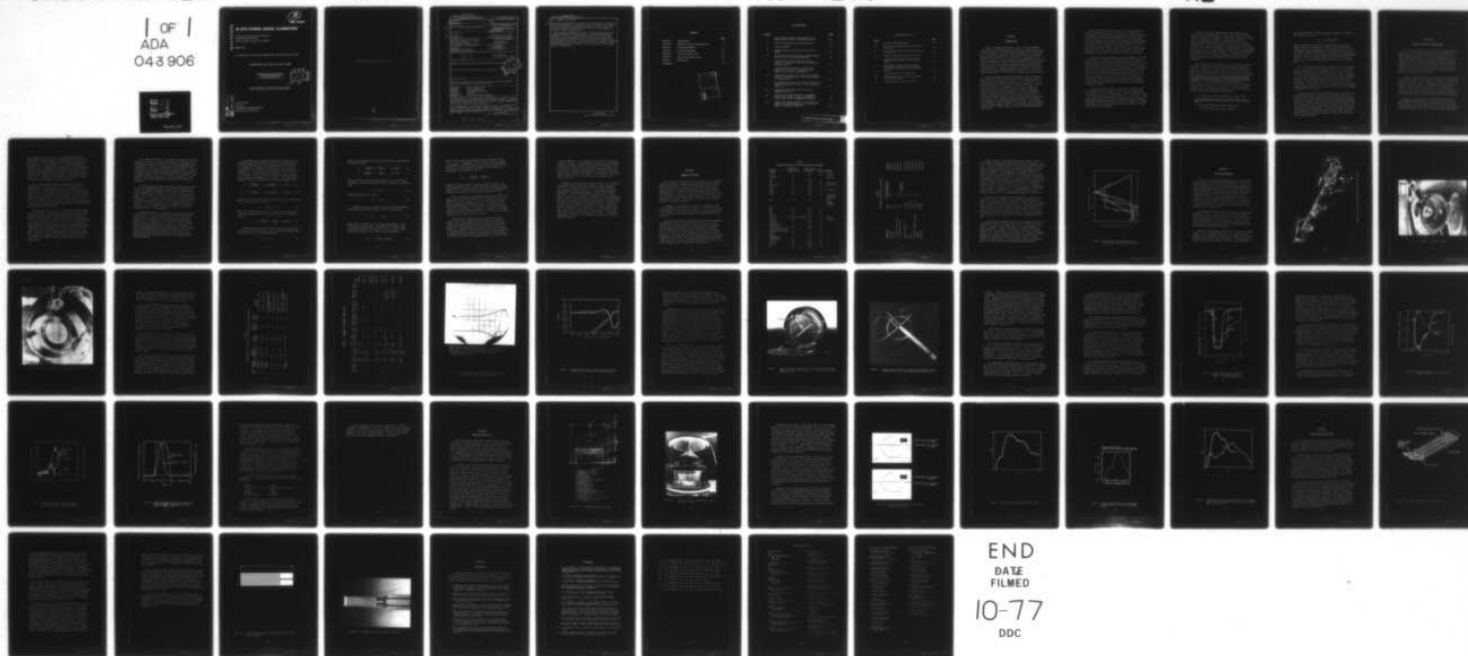
PIFR-755

DNA-4254F

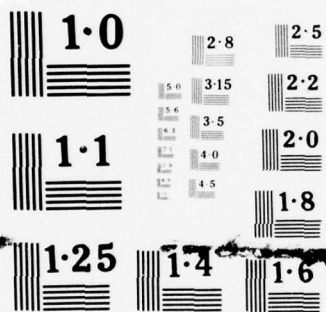
DNA001-75-C-0020

NL

1 OF 1
ADA
043 906



END
DATE
FILMED
10-77
DDC



NATIONAL BUREAU OF STANDARDS
MICROCOPY RESOLUTION TEST CHART

AD A U 43906

12

DNA 4254F

IN SITU STRESS GAUGE CALIBRATION

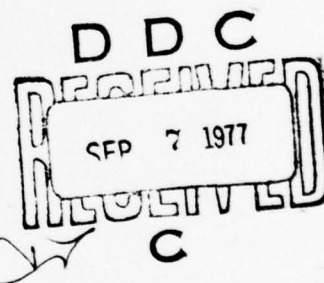
Physics International Company
2700 Merced Street
San Leandro, California 94577

May 1977

Final Report for Period September 1974—February 1977

CONTRACT No. DNA 001-75-C-0020

APPROVED FOR PUBLIC RELEASE;
DISTRIBUTION UNLIMITED.



THIS WORK SPONSORED BY THE DEFENSE NUCLEAR AGENCY
UNDER RDT&E RMSS CODE B344075462 J11AAXSX35218 H2590D.

AU NO. _____
DDC FILE COPY.

Prepared for
Director
DEFENSE NUCLEAR AGENCY
Washington, DC 20305

Destroy this report when it is no longer
needed. Do not return to sender.



UNCLASSIFIED

SECURITY CLASSIFICATION OF THIS PAGE (When Data Entered)

REPORT DOCUMENTATION PAGE		READ INSTRUCTIONS BEFORE COMPLETING FORM
1. REPORT NUMBER DNA 4254F ✓	2. GOVT ACCESSION NO.	3. RECIPIENT'S CATALOG NUMBER
4. TITLE (and Subtitle) IN SITU STRESS GAUGE CALIBRATION	5. TYPE OF REPORT & PERIOD COVERED Final Report, for Period Sep 74 - Feb 77	
7. AUTHOR(s) K./Seifert J./Shea	6. PERFORMING ORG. REPORT NUMBER PIFR-755	
9. PERFORMING ORGANIZATION NAME AND ADDRESS Physics International Company 2700 Merced Street San Leandro, California 94577	8. CONTRACT OR GRANT NUMBER(s) DNA 001-75-C-0020	
11. CONTROLLING OFFICE NAME AND ADDRESS Director Defense Nuclear Agency Washington, D.C. 20305	10. PROGRAM ELEMENT, PROJECT, TASK AREA & WORK UNIT NUMBERS NWER Subtask J11AAXSX352-18	
14. MONITORING AGENCY NAME & ADDRESS (if different from Controlling Office) 126 pp.	12. REPORT DATE May 1977	
	13. NUMBER OF PAGES 62	
	15. SECURITY CLASS (of this report) UNCLASSIFIED	
16. DISTRIBUTION STATEMENT (of this Report) Approved for public release; distribution unlimited.		
17. DISTRIBUTION STATEMENT (of the abstract entered in Block 20, if different from Report)		
18. SUPPLEMENTARY NOTES This work sponsored by the Defense Nuclear Agency under RDT&E RMSS Code B344075462 J11AAXSX35218 H2590D.		
19. KEY WORDS (Continue on reverse side if necessary and identify by block number) In Situ Phase Transition Pressure Bismuth/Lead Alloy Stress Thallium/Indium Alloy Calibration Gas Gun Bismuth Plane Wave Lens, Explosive		
20. ABSTRACT (Continue on reverse side if necessary and identify by block number) The accuracy of <u>in situ</u> stress measurements is dependent upon the presence of strain within the active gauge element. In gauge records of dynamic stress fields, the onset of strain response of the gauge is not able to be defined. Development of a gauge that responds only to the applied pressure, independent of the strain field, is usable in that the deviance of a stress transducer from its calibration in a dynamic		

DD FORM 1 JAN 73 1473 EDITION OF 1 NOV 65 IS OBSOLETE

UNCLASSIFIED

SECURITY CLASSIFICATION OF THIS PAGE (When Data Entered)

282 760

LB


UNCLASSIFIED

SECURITY CLASSIFICATION OF THIS PAGE(When Data Entered)

20. ABSTRACT (Continued)

cont. field can be observed by comparison to the pressure indicated by the calibration gauge. Through the use of variations in resistance or dielectric constant that accompany phase transitions, calibration gauges can be constructed for use in in situ calibration of stress transducers.

The program conducted investigated various materials as candidates for phase transition gauges, including bismuth metal, bismuth/lead alloy (75:25% by weight), thallium/indium alloy, (77:23%). Gas-gun experiments and explosive plane wave lens experiments were conducted during the program with confirmation of the dynamic response of the phase transition; however, accurate determination of the pressure associated with the phase transition and the duration required for the transition to take place was not accomplished.



UNCLASSIFIED

SECURITY CLASSIFICATION OF THIS PAGE(When Data Entered)

CONTENTS

	<u>Page</u>
SECTION 1 INTRODUCTION	5
SECTION 2 MATERIAL PROPERTY CONSIDERATIONS	9
SECTION 3 CANDIDATE MATERIALS	16
SECTION 4 GAS-GUN EXPERIMENTS	21
SECTION 5 PLANE WAVE LENS TESTS	42
SECTION 6 GAUGE FABRICATION EFFORTS	50
SECTION 7 CONCLUSIONS	56
REFERENCES	57

ACCESSION for	
NTIS	White Section <input checked="" type="checkbox"/>
DDC	Buff Section <input type="checkbox"/>
UNANNOUNCED	
S I G N A T U R E	
BY	
DISTRIBUTION/AVAILABILITY CODES	
Di	SPECIAL
A	

ILLUSTRATIONS

<u>Figure</u>		<u>Page</u>
1	Low Pressure Phase Transformations in Metals--Static Data (References 20-22)	20
2	Overview Rendering of Entire Gas Gun	22
3	Target Chamber	23
4	Target-Mounting Ring with Velocity-Pin Block	24
5	Oscilloscope Record Showing Ramped Stress Pulse and Bismuth Gauge Response	28
6	Reduced Data from Third Shot (Quartz Pressure Transducer and a Vapor Deposited Bismuth Gauge)	29
7	Vapor Deposited Bismuth and an Etched Manganin Grid Gauge in Fused Silica Ready for a Gas Gun Experiment	31
8	Bismuth-Lead Alloy Foil Gauge and Manganin Gauge on Fused Silica in the Early Stages of Construction	32
9	Piezoresistance Data for Bismuth (Shot 12), Bismuth-Lead Alloy (Shot 11) and Manganin (Shot 11)	35
10	Piezoresistance Data for Cerium and Manganin--Shot 15	37
11	Capacitance Gauge Record for Ammonium Iodide and Stress in PMMA, as Measured by an X-Cut Quartz Transducer--Shot 17	38
12	Capacitance Gauge Record for Thiourea and Stress in PMMA as Measured by an X-Cut Quartz Transducer--Shot 18	39

ILLUSTRATIONS (cont.)

<u>Figure</u>		<u>Page</u>
13	Explosive Plane Wave Lens	43
14	Plane Wave Lens Experimental Setup, Ready for Firing	44
15	Manganin Gauge Records from Shots ISGC-L2 and ISGC-L3	46
16	Manganin Gauge Record from Shot ISGC-L2	47
17	Computational Results for Experiments; Pressure Shown is Taken at the Gauge Plane	48
18	Experimental Results Plotted Against Computational Results Including Comp-B Pad (Solid Line Represents Experimental Results)	49
19	Phase-Change Gauge Configuration	51
20	Photo Mask Pattern for Phase-Transition Gauge Active Element	54
21	Bismuth Gauge on Sapphire Substrate	55

SECTION 1

INTRODUCTION

Design of hardened underground sites is greatly dependent on the ability to define the impulsive loads to which these sites could be subjected. The amplitudes and durations of these loads are a function of a great many factors including the stress-wave transmission properties of rocks and soils. Knowledge of the dynamic response of soils and rocks has progressed from conjecture, based on hydrostatic studies, through computer calculations and predictions, based on laboratory-generated shock-wave equation-of-state studies. However, the ability to predict site response remains marginally acceptable primarily because of the lack of adequate knowledge of the response of in situ geological materials.

Gross macroscopic characteristics which cannot be studied in laboratory-scale experiments are exhibited by in situ geologic materials and are thought to account for a large portion of the discrepancy between predicted and observed field data. Efforts were initiated in 1970 (Reference 1) to obtain in situ constructive relations from which responses could be predicted. This work relied on the development of suitable "in-material" stress and particle velocity sensors and on the extension of uniaxial Lagrangian analyses of Fowles and Williams to spherically divergent flow. However, Godfrey (Reference 2) has shown, for incompetent (jointed) geological formations, that the concept of determining in situ relations from laboratory-type tangential stress gauges is highly suspect at stress levels below material fracturing.

Geological joints can be the source of a complex array of shear and longitudinal waves. It can also be argued that a consequence of the complex wave propagation in jointed materials is that "radial" stress gauge records may be without meaning since the strength of the material determined by simple constitutive relations from such records may be completely distorted by the effect of joint. However, for competent (not jointed) material such as many playas, tuffs, and alluviums, an in situ technique involving the measurement of particle velocity and stress shows great promise for describing dynamic response.

A current, major limitation to in situ programs is the lack of confidence in field data obtained with stress transducers. Results from piezoelectric and piezoresistance transducers often disagree markedly in stress wave amplitudes. Several suspect areas that may be the cause of such disagreement include calibration standards, transducer emplacement and the effect of both strain rate and strain anisotropy on gauge calibration. The latter is currently thought to be particularly significant in in situ programs, since the stress ranges and durations are significantly lower and longer than obtainable in laboratory calculations and since both types of gauges are susceptible to variations in each.

To apply laboratory derived calibrations to reduce field data requires that the effect of rate and distribution within the gauges must be well characterized. This is a difficult task in the laboratory and particularly difficult in the field. Since in situ programs rely on accurate stress and particle velocity data, either better calibration techniques or greatly increased knowledge of the detailed response of gauge systems to various flow conditions is required.

A number of physical phenomena have been examined with respect to pressure dependence. Primary among these are phase transitions, electrical, magnetic, and optical variations. Review articles (References 3 through 7) summarize the results of pressure-induced changes in electrical polarization, magnetic susceptibility, optical polarization, refractive index, thermoelectric effect, optical absorption, and Hall effect. The response to pressure of all of these but phase transitions is insufficiently defined for use as a pressure standard. The remaining standards are no more clearly defined with respect to strain rate and anisotropy than are piezoresistance or piezoelectric stress transducers.

Work (References 8 through 10) on equating the primary pressure scale obtained from shock loading to that obtained from hydrostatic loading has established an equivalence based on the phase transitions in a number of materials. Jones and Graham have examined shock data for a number of transitions and concluded that the phase transition pressure determined from hydrostatic compression correlates well with the mean hydrostatic pressure calculated from shock experiments for certain materials. Specifically, they have correlated values of specific volume at transition from hydrostatic compression with those calculated from shock data. Correlation to within 0.5 percent in specific volume was achieved for materials exhibiting:

1. An insensitivity of the transition to shear stress
2. Rate-dependent terms for shear corrections to the shock stress data to obtain hydrostatic (or mean pressure) data
3. Well-defined Hugoniot elastic limits (HEL)
4. A limiting shear stress after yielding

For such materials, the mean hydrostatic pressure is related to the uniaxial stress by:

$$\bar{P}_T = \sigma_x^T - \frac{4}{3} \frac{C_s^2}{C_\ell} \sigma_x^{HEL}$$

where C_s and C_ℓ are the shear and longitudinal velocities at ambient pressure, respectively, σ_x^{HEL} is the observed time-independent stress corresponding to the elastic limit, and σ_x^T is the uniaxial stress at transition. This relationship assumes an idealized isotropic, elastic-plastic behavior of the transforming material. However, methods are also described for obtaining σ_x^T and \bar{P}_T in cases of anisotropic materials and an ill-defined HEL.

The significance of correlating hydrostatic and shock data is that the uniaxial phase transition stress, σ_x^T , is a fixed, well-defined quantity for some materials; i.e., it is as much a standard as the hydrostatic transition pressure, \bar{P}_T . Therefore, if the transition stress can be observed by a readily measurable parameter that uniquely describes the transition, the time at which the uniaxial stress attained the specific value can be determined. By comparing the time of transition with the corresponding signal from our stress sensors, we can obtain an in situ calibration for the latter.

The objective of the program conducted was to evaluate the data available concerning pressure-induced phase transitions in materials that would be suitable for utilization as an in situ gauge active element. Upon the selection of suitable materials, testing of these materials in both uniaxial stress dynamic loading environments and in larger-scale divergent shock wave conditions was to be accomplished. Due to gauge physical construction problems, only laboratory-scale uniaxial tests (gas gun experiments) were conducted; however, the viability of the technique was demonstrated.

SECTION 2

MATERIAL PROPERTY CONSIDERATIONS

The basic relationship to be derived from in situ measurements of particle velocity and stress are the constitutive equations relating applied stress to resultant strain. To derive these relationships, an analysis technique was developed by Fowles and Williams in which in-material particle velocity and stress gauges provided experimentally determined Lagrangian functions from which the general flow equations could be solved. From the flow equations, which contain the material velocity and radial and tangential stress, the constitutive relations are calculable.

Ideally, only the particle velocity and radial stress need be measured to completely describe the behavior of the material (assumed competent). The measurement of particle velocity is basically straightforward, although under field conditions it becomes somewhat complicated. However, the measurement of "stress," either radial or tangential is quite difficult, primarily because a resistance change or piezoelectric output is observed and related to stress through a calibration procedure.

Typically, "calibrations" of stress sensors are made in laboratory-scale experiments where the conditions of stress and resulting strain are better understood than in the field. Field uncertainties arise because of the nature of the in situ geological material, the field installation techniques, and

the difference in strain rate. In laboratory calibrations, great care is taken to assure a one-dimensional, uniaxial compression of the stress sensor so that reproducible results can be obtained. In such compression, the resistance change is related to the σ_x component of stress, which is usually obtained from the known, one-dimensional compression characteristics of the material bounding the stress sensor. The stress is applied in times short compared with the lateral transit times of the sensor, i.e., one-dimensional compression is assumed. Unloading response is determined in a similar manner.

The resistance-stress response determined under these compression conditions has been found to vary significantly from hydrostatic compression and also from that in which the strain sensor in the piezoresistance material is greatly varied (Reference 11). Differences on the order of a factor of two are common. In fact, results of manganin calibration under uniaxial static compression (which differs from shock loading only in the rate of stress application) show a coefficient nearly identical to that obtained from hydrostatic compression, but different from the shock-derived uniaxial value.

To overcome the difficulty in calibration techniques, most stress transducers are calibrated using dynamic uniaxial stress generation systems, such as provided by gas guns or high-explosive plane-wave lenses. These calibrations are valid, however, only as long as the stress field to which the gauge package is being exposed remains uniaxial. Since most piezoresistive gauge materials react to induced strain, once tangential strains become present in the stress field, due to the deviation of the shock wave from uniaxial behavior, the usefulness of a gauge ends. Since it is not currently possible to measure accurately the presence of tangential strain under field conditions, the point at which a stress transducer record becomes invalid is questionable.

It is possible, however, to determine the response of stress sensors to the type of loading encountered in field experiments by comparing transducer outputs with a standard pressure calibration system. To do this, a standard must be used that is not susceptible to the same uncertainties as stress sensors. Ideally, a system in which an easily measurable parameter is relatable to a primary pressure scale in an unequivocal way is desired. This parameter could then be used as a stress transducer or in conjunction with stress transducers to determine the response of the latter.

To obtain suitable in situ calibration standards, the possibility that stress references or standards can be obtained by utilizing a correlation between dynamic-shock stress data and a more fundamentally obtained static pressure scale was investigated. The correlation involved is that of a "characteristic" compression, η_T , at which a phase transition in certain materials is initiated, regardless of the type of loading, hydrostatic or uniaxial. Since this transition is independent of strain isotropy and rate, it becomes necessary to relate only applied pressure/stress to the compressibility, η_T .

The applied pressure in hydrostatic loading is that of the medium pressure, a readily measured and/or calculated quantity. In the shock of dynamic uniaxial loading, shear strains are present. It is necessary to know the effects of these shear strains before a comparison with hydrostatic data can be made. Jones and Graham (Reference 8) have shown it is possible to obtain good agreement between the shock-induced stress at phase transition and hydrostatic pressure at phase transition by comparing the mean hydrostatic pressure, P_m^T , existing in the shocked sample and by making a correction for heating due to the shock loading.

To examine how the material properties influence the relationship between the pressure P (which will be determined by the phase transition) and the axial component of the stress, σ_R , consider the following: for simplicity, assume that the orientation of the gauge is in the direction of the principal stresses, and that the transverse stresses, σ_T , and strains, ϵ_T , are equal. During the initial loading the gauge response will be elastic and Hooke's law will apply. The relationship between the axial and transverse stresses and strains is then

$$\sigma_R = \frac{E(1-\nu)}{(1+\nu)(1-2\nu)} \epsilon_R + \frac{2E\nu}{(1+\nu)(1-2\nu)} \epsilon_T \quad (\text{elastic}) \quad (1)$$

$$\sigma_T = \frac{E\nu}{(1+\nu)(1-2\nu)} \epsilon_R + \frac{E}{(1+\nu)(1-2\nu)} \epsilon_T \quad (\text{elastic}) \quad (2)$$

where E and ν are Young's modulus and Poisson's ratio, respectively. The pressure, P , is given by

$$P = -\frac{1}{3} (\sigma_R + 2 \sigma_T) \quad (3)$$

which can be combined with the above equations to yield the relationship between the axial stress, pressure, and transverse strain as

$$\sigma_R = -\frac{3(1-\nu)}{(1+\nu)} P - \frac{2E}{(1+\nu)} \epsilon_T \quad (\text{elastic}) \quad (4)$$

Assuming elastic perfectly plastic material properties and a von Mises yield criterion, for equal transverse stresses yielding will occur for σ_R in compression when

$$\sigma_T - \sigma_R = Y_0 \quad (5)$$

where Y_0 is the magnitude of the yield stress in simple tension.
At the yield point

$$\sigma_R = - \frac{(1-\nu)}{(1-2\nu)} Y_0 + \frac{E}{1-2\nu} \epsilon_T \quad (\text{at yield}) \quad (6)$$

$$P = \frac{(1+\nu)}{3(1-2\nu)} Y_0 - \frac{E}{1-2\nu} \epsilon_T \quad (\text{at yield}) \quad (7)$$

and σ_R and P are still related by Equation (4). For further increases in the compressive axial stress, Equation (5) requires that

$$d\sigma_T = d\sigma_R \quad (8)$$

which with Equation (3) leads to

$$dP = - d\sigma_R \quad (9)$$

Consequently, for continued loading (increasing pressure) such that the stress state remains on the yield surface

$$\sigma_R - \sigma_R^Y = - (P - P^Y) \quad (10)$$

where σ_R^Y and P^Y denote the axial stress and pressure at the point where yielding begins. The stress and pressure at the yield point are given by Equations (6) and (7), which, when combined with Equation (10), lead to the relationship

$$\sigma_R = - P - \frac{2}{3} Y_0 \quad (\text{plastic}) \quad (11)$$

which is identical to the situation for pure uniaxial strain (i.e., $\epsilon_T = 0$). Consequently, the absolute difference between the magnitude of the axial stress and pressure is never greater than $2/3 Y_0$. Upon unloading, the elastic relationships will again apply (in differential form) as

$$d\sigma_R = - \frac{3(1-\nu)}{(1+\nu)} dP - \frac{2E}{(1+\nu)} \epsilon_T.$$

Reverse yielding can also occur upon unloading; whether this will occur depends upon the peak stress and the amount of transverse strain. If reverse yielding does occur, the magnitude of the axial stress will be less than the pressure by $2/3 Y_0$.

Since, in general, the transverse strains are unknown, one cannot always be certain whether the gauge material is in an elastic or a plastic state, or, if it is in an elastic state, what the numerical difference actually is between the axial stress and the pressure. This difference is, however, bounded by the yield strength of the material. Consequently, the ideal phase-transition transducer would have a very low yield strength compared to the stress level of interest.

The application of the calibration system consists of the following: If, assuming uniaxial strain (no transverse strain), the stress computed from the phase-transition gauge agrees with the corresponding stress transducer (ytterbium gauge, for instance), one can be certain that the transducer is reading correctly (at that time) and has not been subjected to transverse strains capable of perturbing its calibration. If on the other hand, the two gauges disagree, the actual stress

is then uncertain. If no unloading has occurred and the phase transition pressure is above the HEL for the phase-change gauge material, the axial stress can be computed from Equation (11). It should be noted that the presence of transverse strain will always tend to decrease the magnitude of the axial stress when plastic behavior begins (Equation 6). For unloading, the situation is less certain, and the stress will be known only to within $\pm 2/3 Y_0$.

To make use of the derived uniaxial stress, it is necessary to establish a time correlation between a stress transducer output and a manifestation that a transition has occurred in the standard or reference material. A conveniently measured parameter is the resistance change at transition, which has been shown to exist in hydrostatic compression for a number of metals. Similar data from shock loading have not been generated and therefore these data became a necessary goal of this program. In addition to measuring the resistance change, it needed to be shown that the transition occurs on time scales compatible with the intended use of the material. For field gauge calibration, this time is on the order of microseconds. Shock data exist which indicate that transitions can occur on the order of nanoseconds. However, similar data were required for suitable standard materials.

SECTION 3

CANDIDATE MATERIALS

The first effort undertaken in the program was a literature search to establish candidate materials suitable for potential use as gauge elements. Ideally, the materials would be conductors with phase transitions occurring at well-established pressure levels. Accompanying the phase transition, a significant change in the material resistivity would be desirable. However, inasmuch as capacitance gauges have been used in past experiments in the field, the initial literature search was not limited to conductive materials.

A summary of the properties of materials examined in the literature search is presented in Table 1. As can be noted from the references for information concerning the phase transitions, P. W. Bridgman is well established as the leading authority in this area.

On the basis of cost, availability, and material properties, the materials shown in Table 2 were selected for evaluation. Some difficulty was encountered in obtaining mercury selenide and the thallium/indium alloy. Both materials are somewhat toxic, with mercury selenide production requiring a precipitation out of solution. After receipt of the materials, it was evident from the strong odor and rapid sublimation that the vapor pressure of both camphor and orthonitrochlorobenzene would preclude their use as a gauge material; thus their inclusion in the list of materials to be investigated was dropped.

TABLE 1
CANDIDATE MATERIALS FOR PHASE TRANSITION SENSORS

<u>Material</u>	<u>Transition Pressure (kbar)</u>	<u>Relative Volume Change $\Delta V/V$</u>	<u>Reference</u>	<u>Comment</u>
Bismuth	26	0.092	19	Conductor
Cerium	7	0.082	13,15	Conductor
Chromium	4	--		Conductor
AgI	2.9	0.165	17	
HgSe	7	0.097	13,18	Semiconductor
$\text{KB}_5\text{O}_8 \cdot 4\text{H}_2\text{O}$	3.5	0.046	15	Piezoelectric
KClO_3	7.5	0.057	16	
KNO_3	3.6	0.102	17	Ferroelectric
NH_4CHO_2	11.2	0.120	15	
PbI_2	5.0	0.040	15	Single XTAL, σ depends on orientation
NH_4I_2	0.5	0.141	17	Pressed powder, $\sigma_0 = 1.9 \times 10^7$ $(\Omega\text{-cm})^{-1}$
RbB_r	4.5	0.138	17	
RbCl	4.9	0.144	17	
RbI	4.0	0.130	17	
Teflon	6.4	0.025	15	
75Bi/25Pb	25 loading/4.9 unloading	0.007	20	Conductor
77Tl/23In	11.5	0.006	21	Conductor
d-Camphor	3.5	0.052	15	
Methyl-amine hydrochloride	5.4	0.054	15	
Ortho-nitrochlorobenzene	3.9	0.007	15	
Para-aminobenzenesulfonic acid	3.9	0.011	15	
Quinone	4.4	0.002	14	
Semicarbazide hydrochloride	9.3	0.003	15	
Nitrourea	5.4	0.059	15	
Thiourea	3.5	0.021	15	
Urea	5.4	0.067	15	

TABLE 2
MATERIALS SELECTED FOR TESTING

<u>Material</u>	<u>Form</u>	<u>Nominal Transition Pressure (kbar)</u>	<u>Comment</u>
Bismuth	foil	25	metallic
Cerium	foil	7	metallic
77 Thallium/23 Indium	foil	11.5	metallic
75 Bismuth/25 Lead	foil	25 (loading) 4.9 (unloading)	metallic
Mercury Selenide	powder	7	semimetal
KNO ₃	crystals	3.6	dielectric
NH ₄ I ₂	crystals	0.5	dielectric
Ortho-nitrochlorobenzene	crystals	3.9	dielectric
Camphor	powder	3.5	dielectric
Thiourea	powder	3.5	dielectric

A graph (compiled from References 20-22) of the relative resistance of the candidate metallic materials is presented in Figure 1. While the behavior of the thallium/indium alloy and cerium metal is rather straightforward, the behavior of the two bismuth bearing candidates is more complex. Pure bismuth exhibits a dramatic increase in resistance under increasing load, up to the point of the first phase transition. At that point a marked drop in resistance to about 0.25 of its initial resistivity occurs. This is associated with the transition from bismuth I to the bismuth II state. As the pressure continues to increase, the transition from the bismuth II state to the bismuth III state is accompanied by an increase in the resistivity to approximately 0.7 times the initial value. Unloading of the pure bismuth sample occurs along the same path as the loading phase/resistivity transitions.

Bismuth/lead (75 percent to 25 percent) alloy does not exhibit the variety of phase transitions along the loading path; however, its unloading path is markedly different from its loading path. Whereas the phase transition and its associated resistivity change occurs at around 25 kbars on loading; upon unloading, it does not occur until the pressure has been reduced to 4.9 kbars. This behavior makes the bismuth/lead alloy quite interesting for a phase-transition calibration gauge in both loading and unloading.

The nonmetallic candidate materials were examined for use as capacitance gauges for in situ tests. In this role, with the increase of pressure, and at some point with the occurrence of a phase transition, a change in dielectric constant was expected. Additionally, corresponding to each phase transition was an abrupt change in the specific volume of the material. These two effects, volumetric and dielectric constant changes, should be complementary and should result in a significant change in the capacitance of a gauge under the loading conditions anticipated.

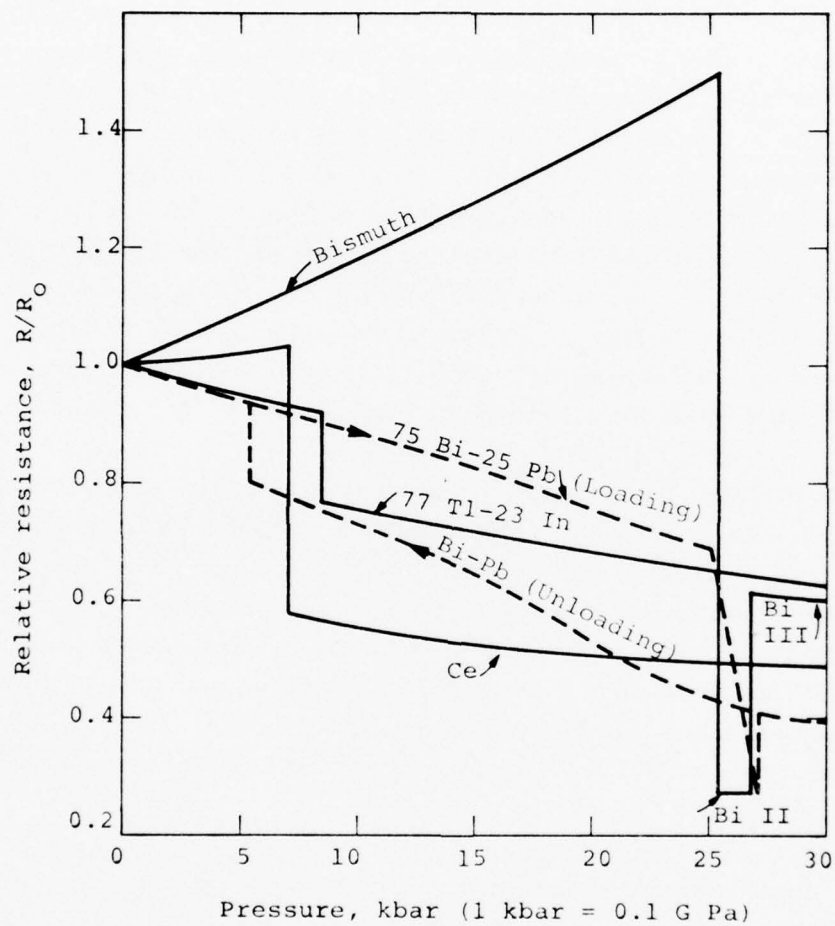


Figure 1 Low pressure phase transformations in metals--static data (References 20-22).

SECTION 4

GAS-GUN EXPERIMENTS

Early in the program, the desirability of a stress wave with a relatively long risetime was identified. With a long risetime pulse, the ability of the experimental technique to verify the pressure at which a phase transition takes place becomes somewhat more reliable. A very fast risetime would require quite precise data recording techniques to be able to accurately observe the onset of a phase transition and correlate it with the pressure in the medium at that time. Additionally, the period of time necessary for a phase transition to occur was unknown, and high accuracy in the data recording system would be negated by a significant time requirement for phase transition.

To evaluate this long risetime requirement and the phase transition duration, it was decided to utilize the Physics International 4-inch light gas gun. The use of this facility would allow rapid turn around for testing, as well as cost effective experiments. Figure 2 shows an overall sketch of the gas the gas gun facility. Note that both ends of the gun are enclosed in concrete block houses.

Targets for these tests were placed in the target chamber, Figure 3, and the chamber evacuated to 50 microns or less. A closeup view of the target mounting ring is shown in Figure 4. Alignment of the target with the surface of the impacting flyer plate was accomplished through the use of a dial indicator

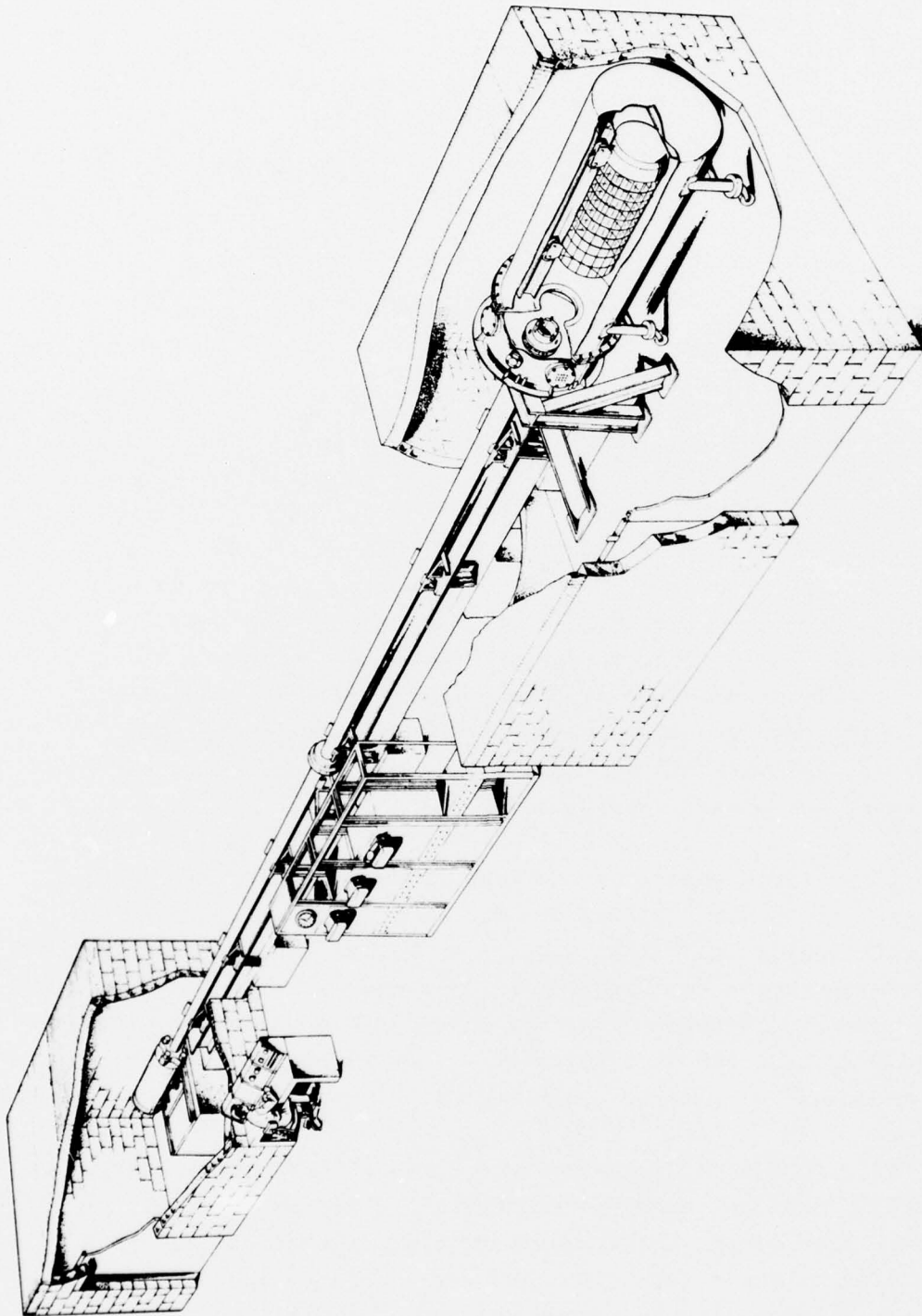


Figure 2 Overview rendering of entire gas gun.

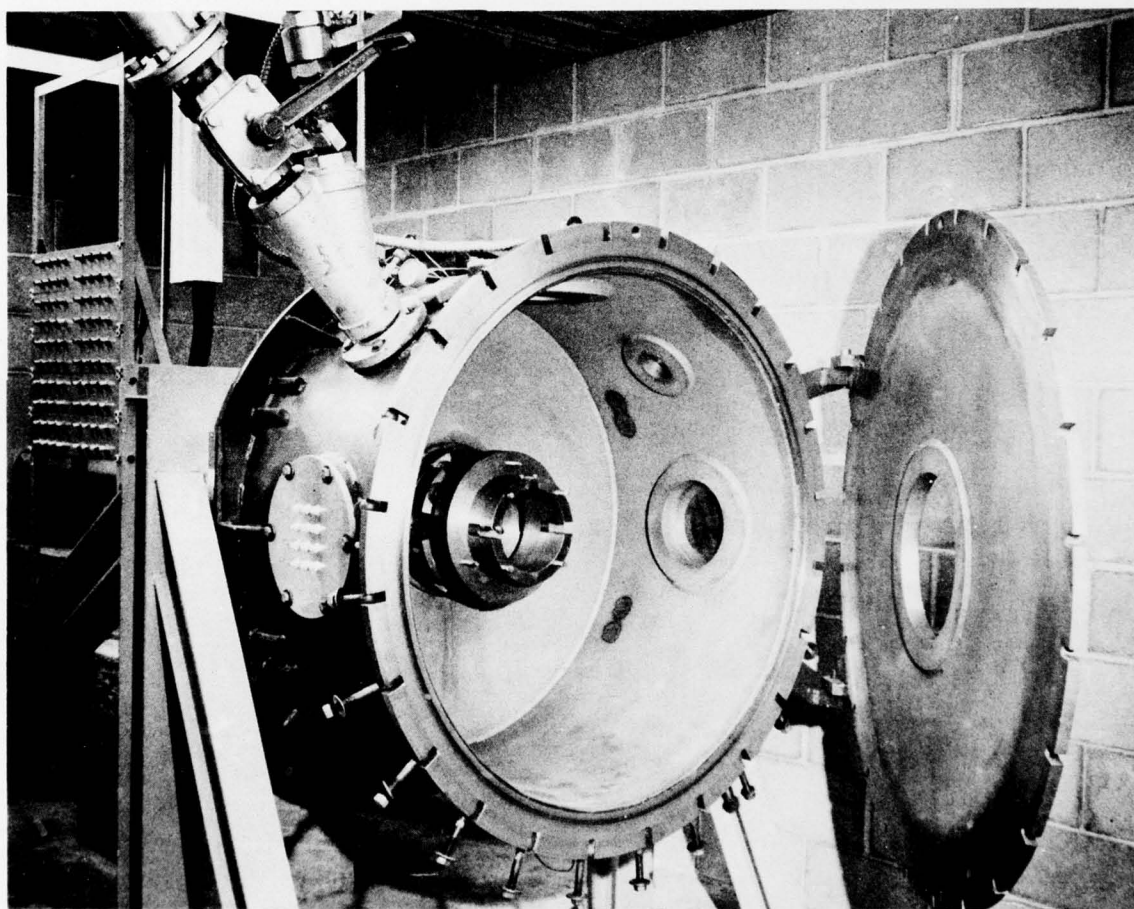


Figure 3 Target chamber.

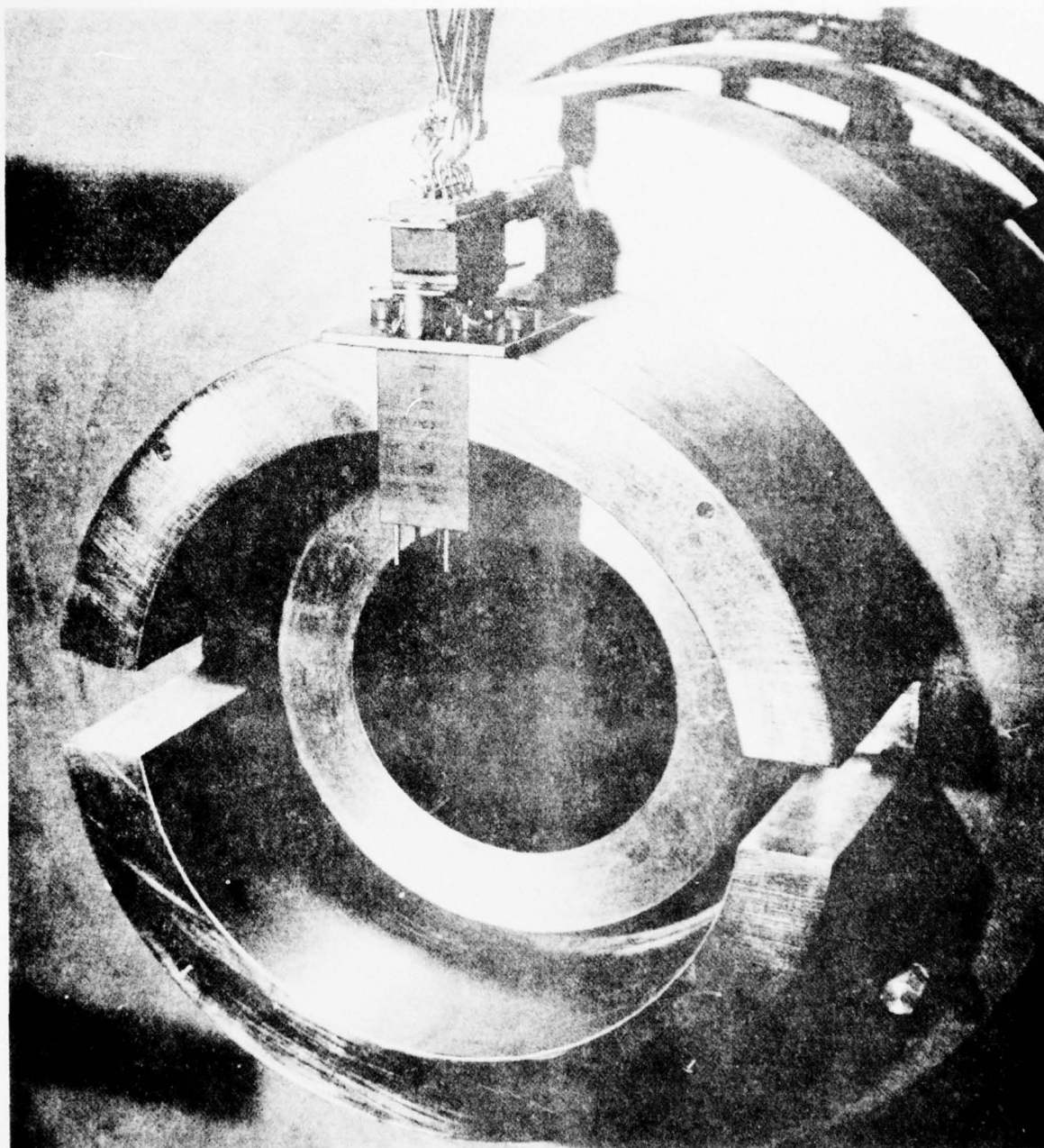


Figure 4 Target-mounting ring with velocity-pin block.

mounted on a ground surface plate. The orientation of the projectile was noted and maintained in the breech chamber during the loading operation. This method allowed projectile/target interface misalignment of less than 1 mrad typically.

Two gas-gun shots were fired to evaluate the use of sintered bronze to obtain a ramped stress pulse suitable for phase change pressure determinations. The stress pulse obtained in the experiments did not provide the desired stress wave shape. Further work indicated that the dispersive nature of fused quartz could be utilized. A fused quartz configuration was designed and tested on a subsequent gas gun shot. A nearly linear ramp was obtained with a nominal duration of 0.8 μ sec. An X-cut quartz transducer was used to measure the stress pulse. Tables 3 and 4 summarize the gas-gun experiments conducted on this program.

The configuration that was planned for use in evaluating candidate (resistive) calibration gauge materials was tested on the same shot that was used to verify the stress wave shape from fused silica. A vapor-deposited bismuth gauge was sandwiched between the fused silica and the quartz transducer. An oscilloscope record showing both the quartz and bismuth gauge responses is shown in Figure 5. The peak stress obtained by the impact was 32.4 kbars.

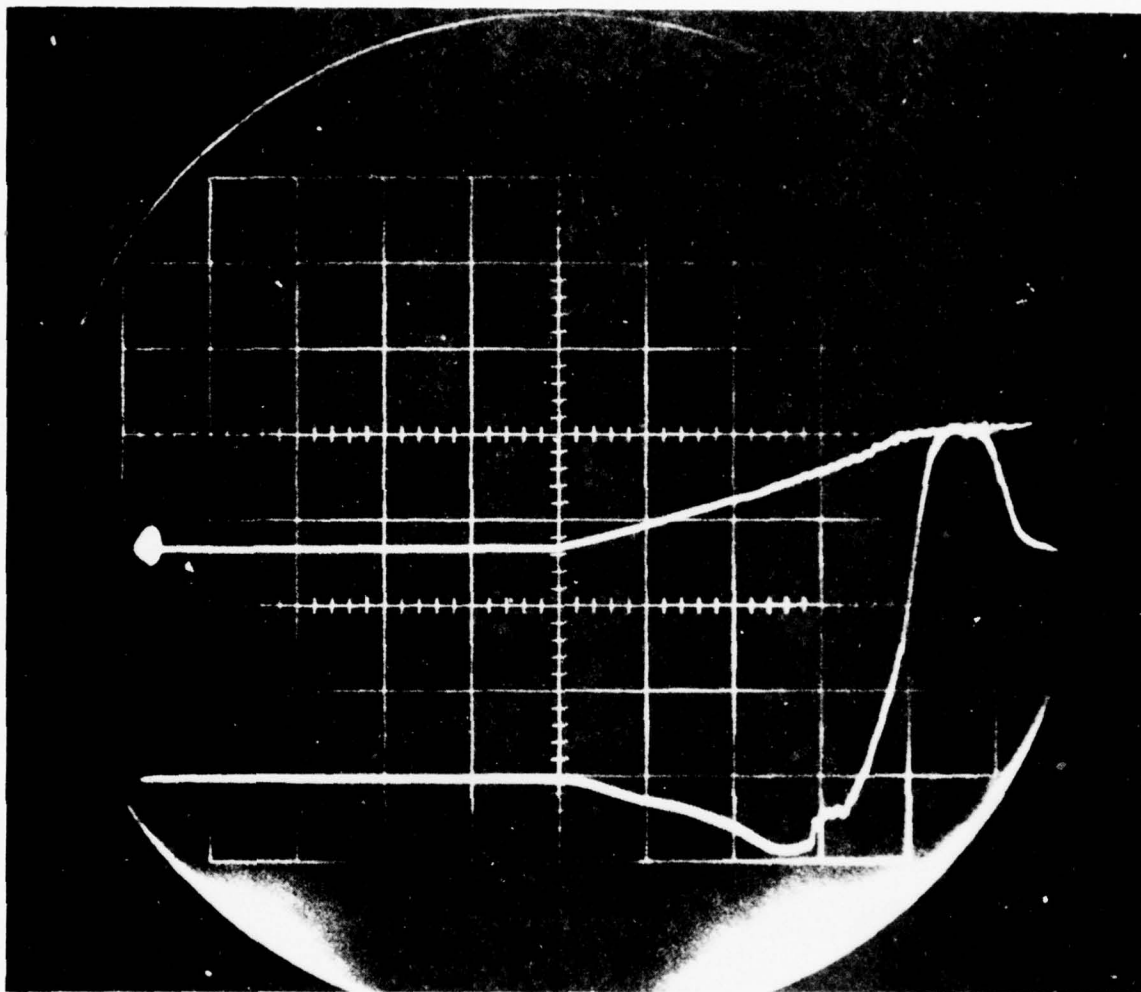
The bismuth gauge record showed the nominal response anticipated and is presented in Figure 6. The resistance increased initially, dropped substantially (bismuth I to bismuth II) and then increased (bismuth II to bismuth III). The quantitative correlation with the quartz transducer record, however, was not as good as might be hoped, which may be attributed to several factors. First, the projectile tilt on the shot (1.3 mrad) was considerably larger than normal, thus tending to smear out the

TABLE 3
SHOT SUMMARY OF INITIAL GAS GUN EXPERIMENTS ON TEST MATERIALS

Shot No.	Gauge Material	Target Material/ Configuration	Flyer Material	Impact Velocity (mm/usec)	Peak Stress (kbar)	Result
3	Bismuth/ quartz	Fused silica	Aluminum	0.48	32.4	Bi-transitions observed
4	Bismuth/ quartz	Fused silica	Aluminum	0.48	32	Bi-gauge broke up early
5	Cerium/ quartz	Fused silica	Aluminum	0.179	14.6	No transition observed, gauge broke up at peak stress level
6	Cerium	PMMA	Aluminum	0.334	10	Shock arrival observed, no transition
7	Tl-In	PMMA	Aluminum	0.49	14.5	Power supply failed to trigger
8	Tl-In	PMMA/C7 epoxy	Aluminum	0.49	14.5	Shock arrival ambiguous, no transition observed
9	Bi-pb/ manganin	Fused silica	Steel/Delrin	0.34	30.0	Transitions observed

TABLE 4 SUMMARY OF IMPACT CONDITIONS

Shot No.	Impact Velocity (mm/usec)	Flyer Plate Material	Buffer Plate Material(s)	Phase Change #1 Material	Phase Change #2 Material	Stress Gauge	Maximum Risettime Due to Tilt Across Phase Change Gauge	Maximum Risettime Due to Tilt Across Stress Gauge	Maximum Stress Observed by Stress Gauge	Design Stress (kbar)	Remarks
11	0.334	304 Stainless Steel	Fused Silica $\frac{1}{4}$ in.	75 Bi/25 Pb Alloy	N/A	Manganin	0.030 μ sec	0.025 μ sec		30	Resistance Change Gauge
12	0.325	304 Stainless Steel	Fused Silica $\frac{1}{4}$ in.	Bismuth	N/A	Manganin	0.012 μ sec	0.004 μ sec		30	Resistance Change Gauge
13	0.354	Aluminum	PMMA $\frac{1}{4}$ in.	HgSe	N/A	N/A	0.021 μ sec	N/A	N/A	10	Gauge Record Very Noisy; Resistance Change Gauge
14	0.182	304 Stainless Steel	Fused Silica $\frac{1}{4}$ in.	0.77 Ti/23 In. Alloy	N/A	Manganin	0.025 μ sec	0.016 μ sec	11.4	15	Resistance Change Gauge
15	~ 0.5	Aluminum	PMMA $\frac{1}{4}$ in.	Cerium	N/A	Manganin	0.23 μ sec	0.009 μ sec	10.7	15	Resistance Change Gauge
16	0.593	304 Stainless Steel	Sintered Bronze, $\frac{1}{4}$ in. PMMA $\frac{1}{4}$ in.	KNO ₃ (Potassium Nitrate)	Epon 202 Epoxy	Quartz, 1 μ sec	0.046 μ sec	0.032 μ sec	Gauge Broke up Before Peak Stress Observed	10	Capacitance Change Gauge
17	0.572	304 Stainless Steel	Sintered Bronze, $\frac{1}{4}$ in.; PMMA, $\frac{1}{4}$ in.	NH ₄ I (Ammonium Iodide)	Teflon	Quartz	0.013 μ sec	0.010 μ sec	Exceeded Recording Time Before Peak Reached	10	Capacitance Change Gauge
18	0.501	304 Stainless Steel	Sintered Bronze, $\frac{1}{4}$ in.; PMMA, $\frac{1}{4}$ in.	NH ₂ SCNH ₂ (Thiourea)	Epon 202 Epoxy	Quartz	0.016 μ sec	0.011 μ sec	11.2	7	Capacitance Change Gauge



Sweep speed: 0.2 $\mu\text{sec/div}$
Upper trace: Quartz gauge record, 25 kbar/div
Lower trace: Bismuth gauge record, 23% resistance
Charge/division (upward deflection indicates
decreasing resistance)

Figure 5 Oscilloscope record showing ramped stress pulse and bismuth gauge response.

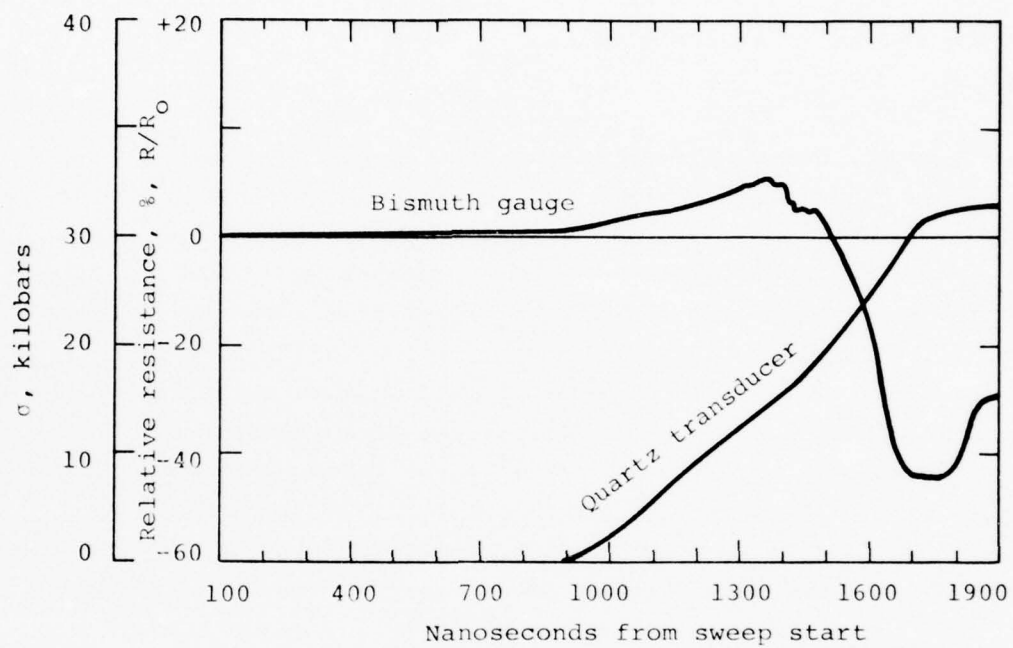


Figure 6 Reduced data from third shot (quartz pressure transducer and a vapor deposited bismuth gauge).

transition. Moreover, the bismuth gauge extended somewhat beyond the edge of the quartz gauge, so the stress in that portion of the gauge would be considerably less (since it was backed by epoxy rather than quartz). Finally, some difficulty had been encountered in obtaining good electrical contact with the bismuth.

Improvements were made in the lead attachment quality, and the gauge design was modified to keep the active element in the same one-dimensional response region as the active portion of the quartz gauge. Subsequently, two attempts were made to demonstrate the validity of this configuration. On the first shot, the oscilloscopes were triggered prematurely by a malfunction in the firing chassis, and no data were obtained. On the second shot, the bismuth gauge appeared to short out early in the pulse (at a few kbars); the quartz gauge record was valid. The reason for the bismuth gauge failure was not understood. It is difficult to fathom how an impact-produced short could occur with the particular target configuration used. It is believed that the crowbar circuit of the power supply was the source of the failure.

In the initial experiments on bismuth and cerium, a thick fused silica target was used to obtain a ramped stress pulse ($\sim 0.8\text{-}\mu\text{sec}$ risetime) at the location of the test material; an X-cut quartz transducer ($1.0\text{-}\mu\text{sec}$ reading time) that backed the test material provided a time-resolved confirmation of the stress history. This configuration led to several difficulties. First, the 1.0-inch-thick fused-silica target (needed to obtain the stress ramp) limited the time interval during which uniaxial strain conditions were maintained at the test material location. The 1-inch-diameter quartz gauge also introduced stress perturbations shortly after its $1\text{-}\mu\text{sec}$ reading time limit was reached, thus preventing observations of the unloading of the test

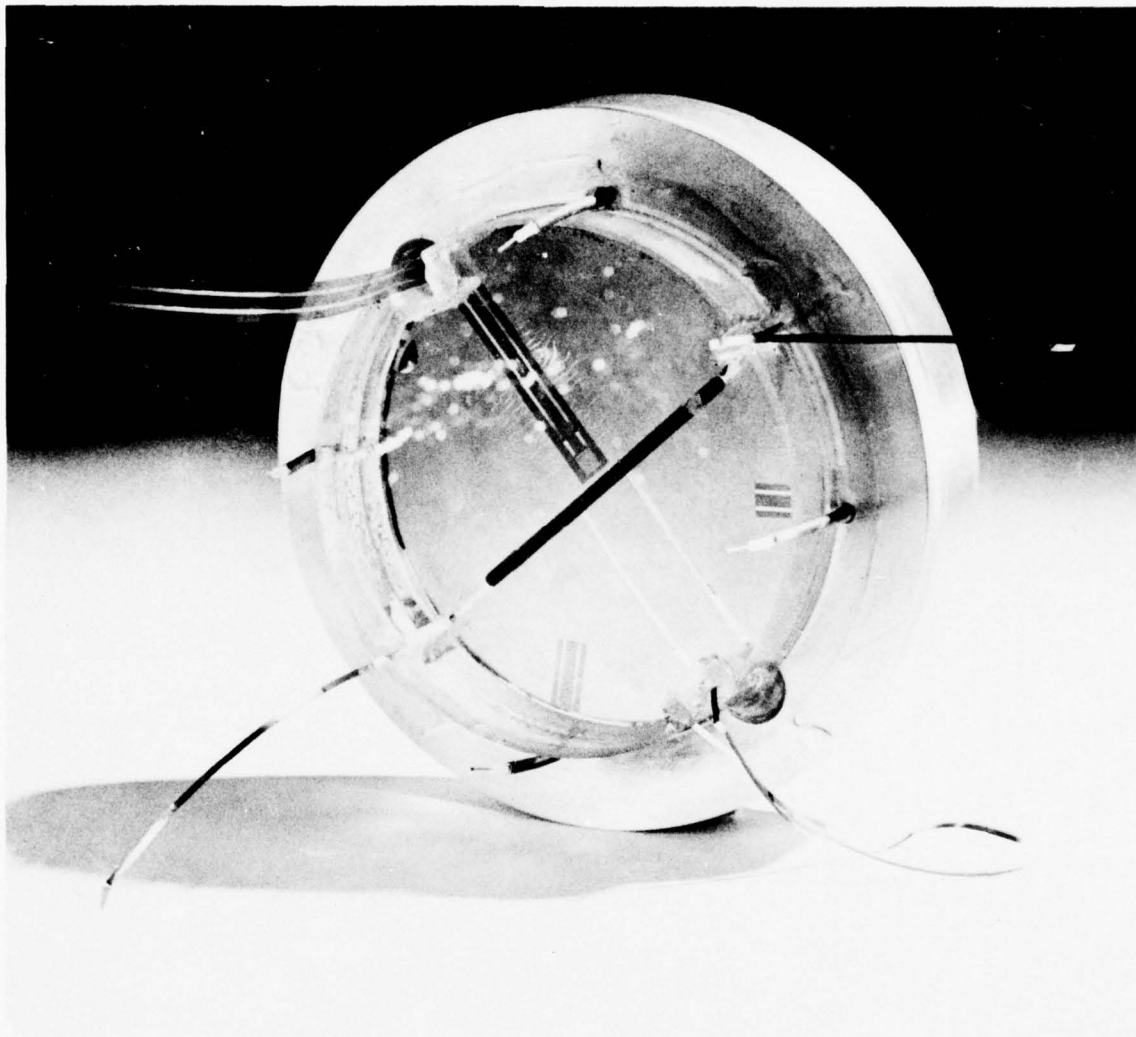


Figure 7 Vapor deposited bismuth and an etched manganin grid gauge in fused silica ready for a gas gun experiment (Shot No. 12).

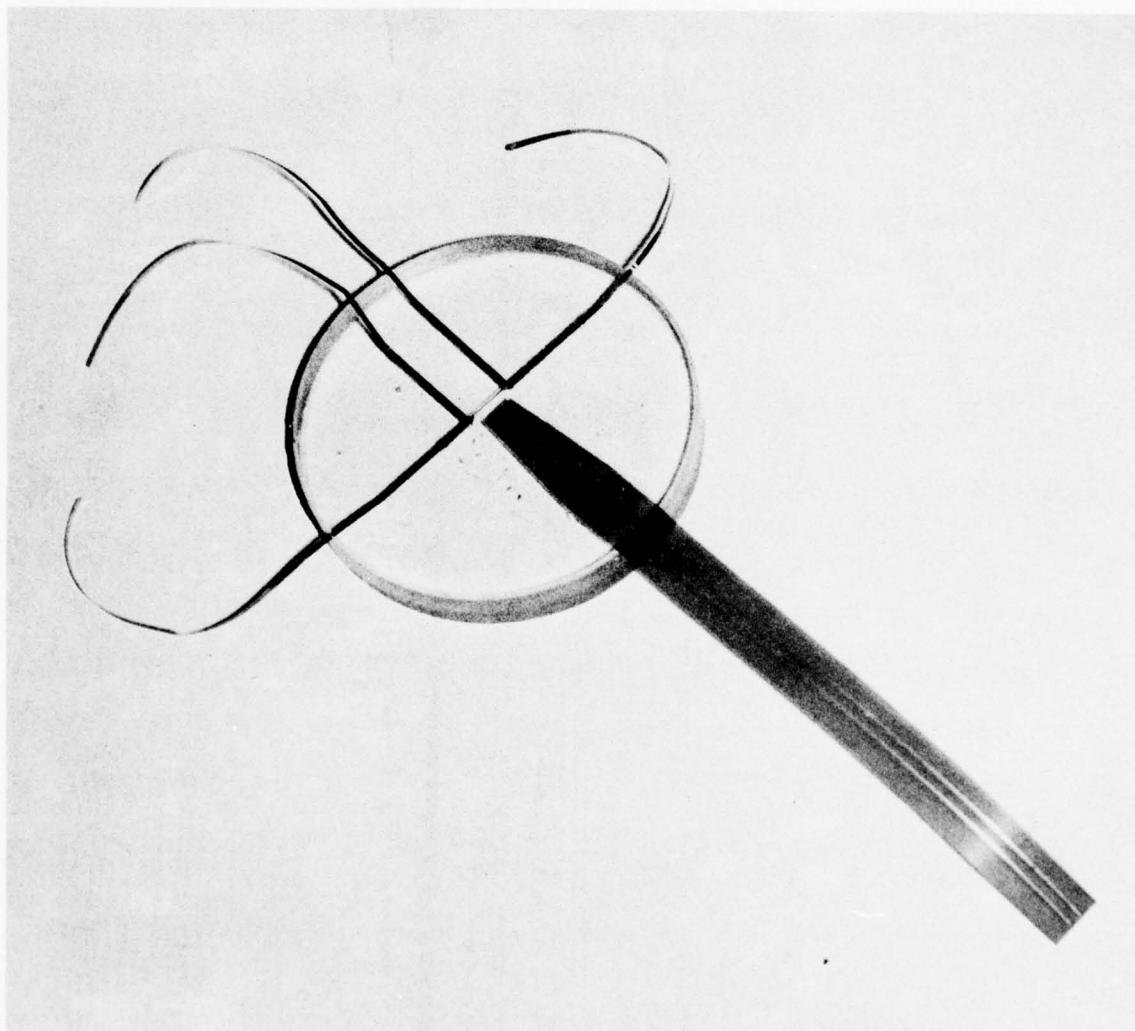


Figure 8 Bismuth/lead alloy foil gauge and manganin gauge on fused silica in the early stages of construction.

material. Finally, it was difficult to make electrical lead attachments to the test material that would survive the complex stress loadings where they emerged from underneath the quartz gauge. Therefore, after the first cerium gauge failed to show the expected transition immediately upon arrival of the stress pulse, subsequent experiments were simplified to obtain longer duration "flat-topped" stress loading to establish whether the transformations occur (at least within a few microseconds). Subsequent experiments could then be used to establish the precise stress. Figure 7 shows a vapor deposited bismuth gauge with a manganin etched grid gauge along side in the longer-duration configuration. Figure 8 illustrates the mounting of a bismuth/lead alloy foil gauge on a fused silica disk in the early stages of construction.

The failure of the cerium (shots No. 5 and 6) to undergo the 7-kbar level transformation during the 2- to 3- μ sec stress duration is surprising, especially since the static transformation is attributed to an electronic transition (4f to 5d), and does not require an atomic rearrangement.

The thallium-indium gauge (shots No. 7 and 8) turned out to have a very low resistance (0.25 ohm) and consequently the signal levels achieved were rather low. However, a resistance change equal to the static transition value should have been detectable. It is believed that the shock arrival is just discernible in the experimental traces; however, the magnitude is lower than expected, neglecting the transformation.

The experimental configuration for the bismuth/lead alloy was modified to distinguish the behavior between loading (25-kbar transition) and unloading (5-kbar reverse transition). A steel flyer was used with a fused-silica target so that the initial peak stress would "ring down" in steps. A manganin gauge was co-located with the bismuth/lead for correlation.

In all subsequent tests for the piezoresistive gauges, the flyer plate was selected to have a greater acoustic impedance than the target so that the stress would ring down from its peak value. The stress at which phase transformations occur on unloading should be more readily determined in such a case. For the capacitance gauges, where the anticipated phase transformations are at relatively low stresses (< 10 kbars), a sintered bronze buffer was used between the flyer plate and the gauge in order to obtain dispersion of the shock wave.

The capacitance gauges were fabricated by grinding the dielectrics (except teflon) to a fine powder, mixing it with Furane Epocast 202/9652, and casting the mixture into a thin slab which was nominally 0.006 inch thick. The dielectric was sandwiched between two vapor-deposited conductive layers.

Good results were obtained on the bismuth, bismuth/lead alloy, cerium, and thiourea gauges. The results obtained on the ammonium iodide were encouraging. The mercury selenide gauge apparently indicated a phase change; however, the record was quite noisy. An extremely small signal was seen for the thallium/indium alloy due to the very low initial resistance of the gauge (0.16 ohm); however, the signal obtained does indicate a change in resistance of between 10 and 20 percent, which is consistent with static data. Poor results were obtained on teflon and potassium nitrate; no appreciable response was seen with the Epon 202 epoxy.

The results obtained with the bismuth and bismuth/lead (75:25) alloy are shown in Figure 9. The manganin gauge record obtained concurrently with the bismuth/lead alloy is superimposed on the data. The impact velocity for the bismuth gauge shot was within 3 percent of that for the bismuth/lead alloy shot. These results show several important features. First, the bismuth

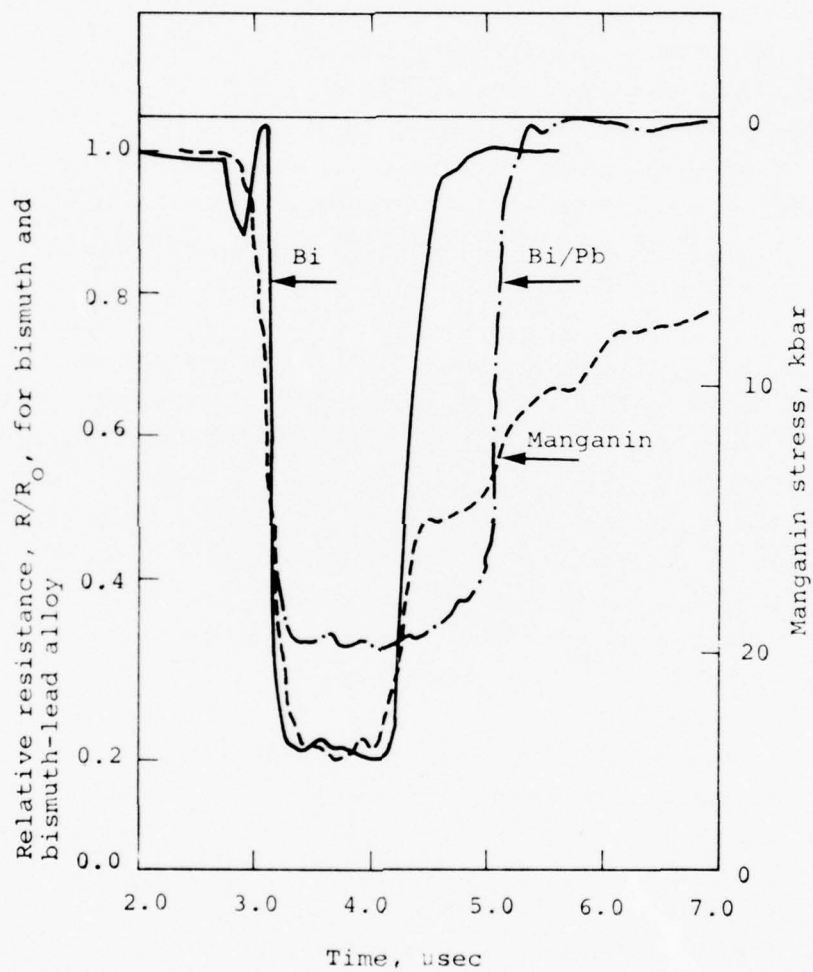


Figure 9 Piezoresistance data for bismuth (Shot 12), bismuth-lead alloy (Shot 11) and manganin (Shot 11).

gauge shows the bismuth I to bismuth II transition (25 kbar nominal), which reverses at the same time the manganin gauge drops from its peak value. The alloy, however, does not undergo the reverse transition until the stress drops to approximately 13 kbars. Bridgman's static data (Reference 20) indicate 5-kbar value for the reverse transition; it is not known what this discrepancy is due to, however two possibilities are rate effects and non-hydrostatic stress states. Nevertheless, presence of the reverse transition in this pressure range would be quite useful in an in situ stress calibration gauge, especially since it applies to the unloading.

The data obtained with the cerium gauge are presented in Figure 10, along with a manganin gauge record obtained concurrently. The improvement in results obtained with this gauge over previous attempts probably relates to modifications in the technique used to obtain electrical connections to the cerium. The initial cerium response observed is an increase in resistance (as it should) followed by an abrupt drop as the phase transformation occurred. The reverse transition is seen to occur near the 7-kbar level as expected from static data.

The results obtained on ammonium iodide are shown in Figure 11. The ammonium iodide record is somewhat noisy. However, an abrupt change in voltage can be discerned at a stress (in PMMA) between 0.5 and 1.0 kbar (comparing with the concurrent quartz gauge record). A transition at 0.5 kbar is predicted from static data. The source of the voltage change 1 μ sec later has not been identified. Note, however, that the valid reading time of the quartz was limited to 1 μ sec.

The thiourea data are shown in Figure 12, along with a quartz gauge record obtained concurrently. The data were obtained only on a relatively slow sweep scope. Consequently,

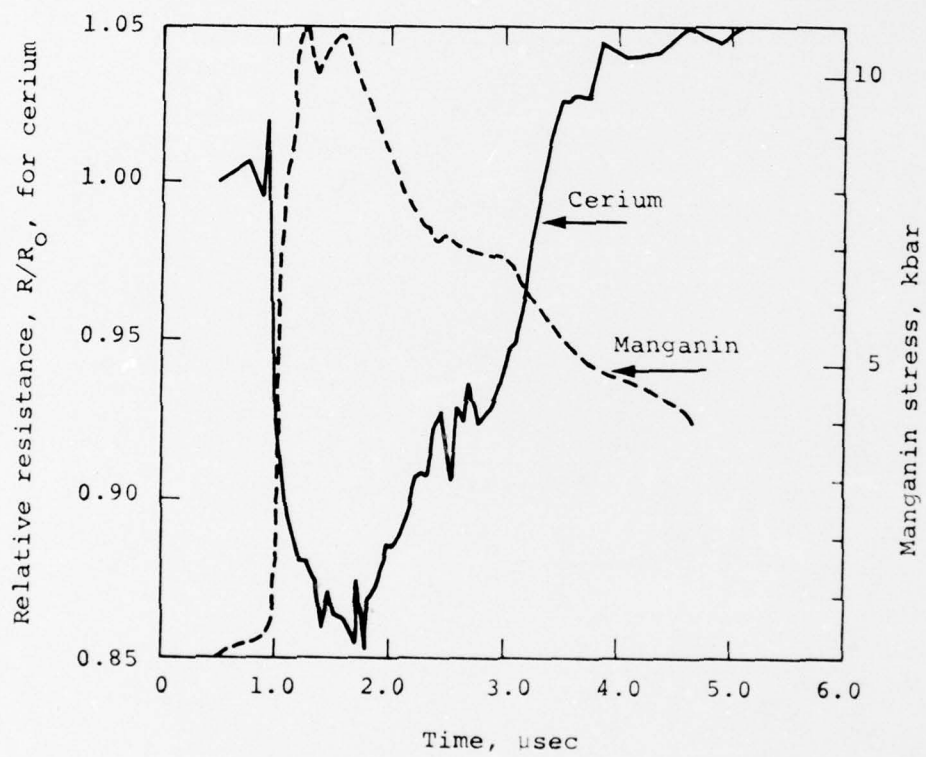


Figure 10 Piezoresistance data for cerium and manganin--Shot 15.

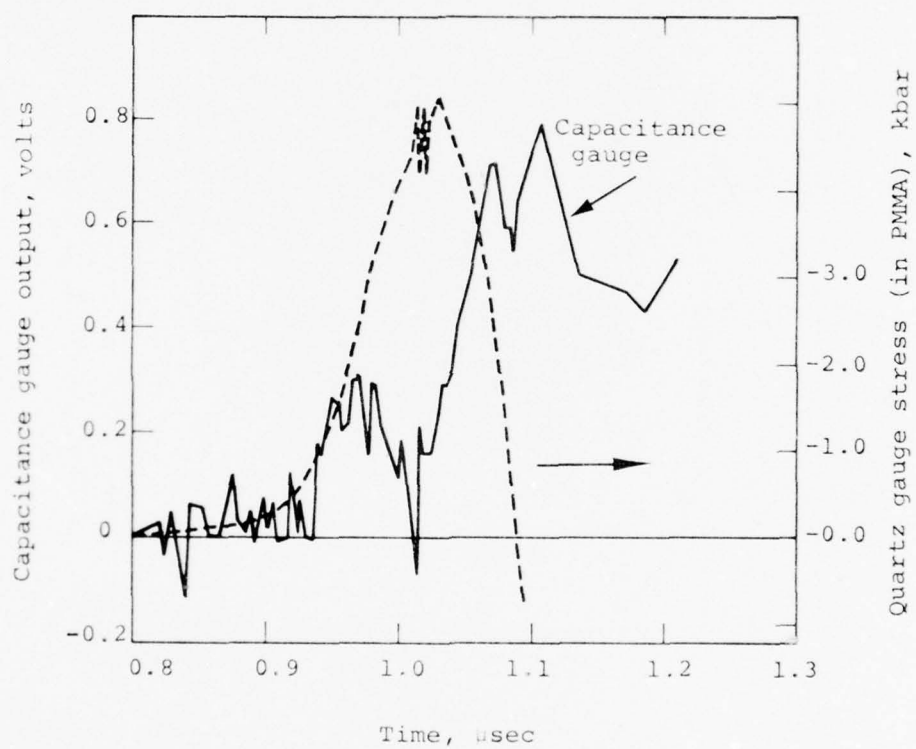


Figure 11 Capacitance gauge record for ammonium iodide and stress in PMMA, as measured by an X-cut quartz transducer--Shot 17.

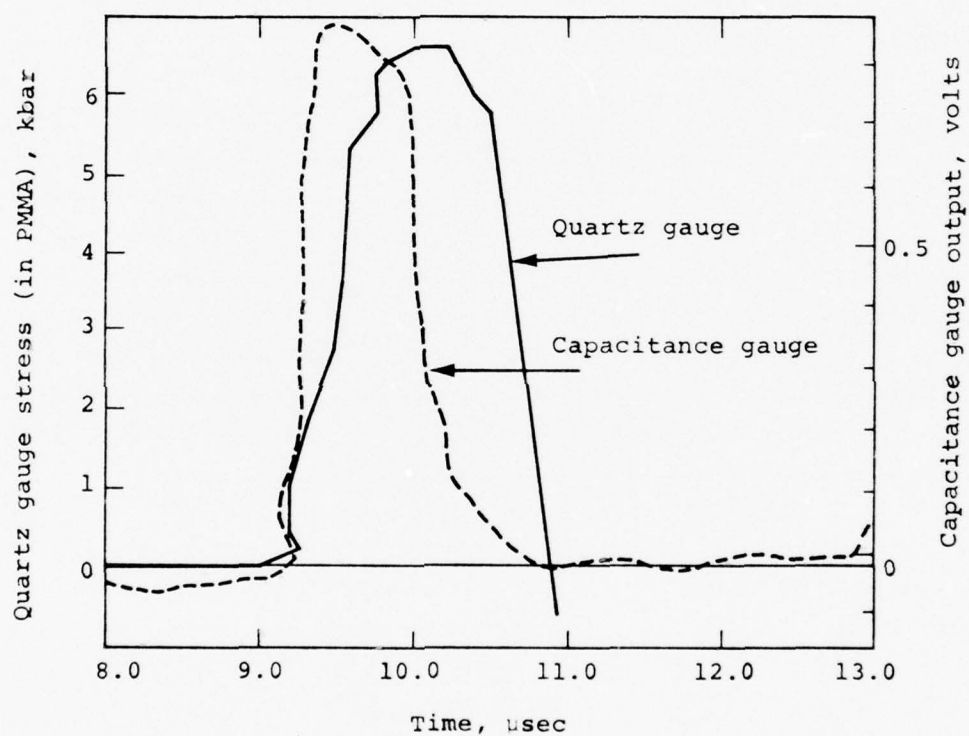


Figure 12 Capacitance gauge record for thiourea and stress in PMMA as measured by an X-cut quartz transducer--Shot 18.

the digitization process produced some rather unphysical distortions of the records (which appear smooth to the eye in the original). From static data a transition was expected at 3.5 kbar. The risetime of the pulses and uncertainties in arrival time are such that it is not possible to discern a specific stress at which the voltage change occurred. However, the signal was clear and was very likely near the static value. Again, it should be borne in mind that the quartz gauge read-time was limited to 1 μ sec.

Subsequent close examination of the capacitance gauge data and the electronic circuitry utilized in the gas-gun tests revealed that the data obtained were not a true representation of capacitance change occurring at the phase transition pressure. The particular combination of capacitance obtained in the manufacture of the gauge and the resistor used as a current viewing resistor combined in parallel to yield an "RC" time so short as to be not observable with the sweep rates used in the experiments. Accordingly, the data observed represent some phenomenon other than capacitance change.

At the conclusion of the gas-gun tests, several viable candidates for an in situ calibration gauge had been identified. These were:

Bismuth	25 kbars
Bismuth/Lead (75:25)	25 kbars/5 kbars unloading
Cerium	7 kbars
Thiourea	3.5 kbars
Ammonium Iodide	0.5 kbar

Mercury selenide could prove to be a useful candidate; however, its toxicity makes it quite difficult to handle. Additionally, its cost and availability is somewhat less than desirable; consequently, its investigation was dropped in favor of more likely candidates.

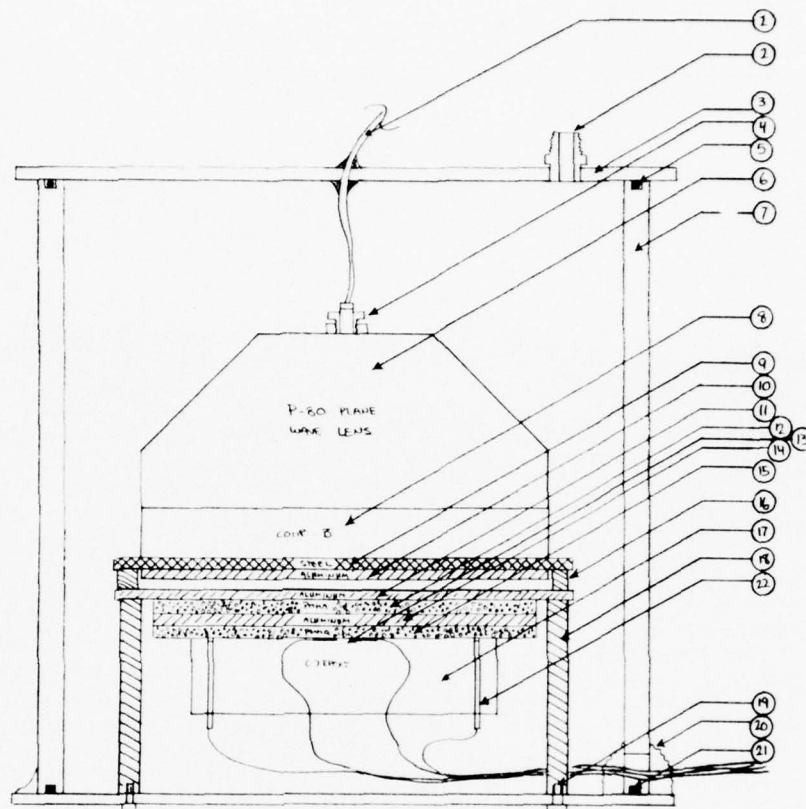
The thallium/indium alloy (77:23) appears to be a useful candidate. Unfortunately, it is quite conductive, and an adequate evaluation will require an etched grid pattern to obtain a more workable value for the gauge resistance. Thallium is also somewhat toxic, which may represent handling difficulties.

SECTION 5

PLANE WAVE LENS TESTS

While light-gas-gun shots were sufficient to verify the usefulness of candidate materials from a qualitative standpoint, they did not yield the necessary resolution to identify the actual phase-transition pressure under dynamic conditions. Better resolution could only be obtained through the attainment of a longer risetime on the pressure pulse. To accomplish this, a set of experiments was performed utilizing plane wave lenses to observe the phase transitions with greater resolution. The configuration for these experiments is shown in Figure 13.

A P-80 plane wave lens was used to generate a planar shock wave in a steel plate. The shock propagated into an aluminum plate and, after its reflection at the free surface of the aluminum, caused the aluminum plate to be launched from the steel as a result of its higher particle velocity. The aluminum plate then impacted a laminate of alternating aluminum and polymethylmethacrylate (PMMA) layers. The gauges (consisting of manganin, carbon) and the materials to be evaluated were located between the last PMMA layer and a C-7 epoxy backing. The intent of the design was to use the impedance mismatches and multiple reflections between the aluminum and PMMA to attenuate the leading portion of the stress pulse and to increase the risetime. By allowing the impacting aluminum plate to have a free run, it was hoped that the decreasing portion of the pulse could be observed during the one-dimensional response time available at the site of the gauges. Based upon pretest finite difference computations, a peak pressure of 30 kbar was anticipated for this configuration. Figure 14 shows the experimental setup ready for firing.



PARTS LIST

- 1- DET. CABLE, EPOXY INTO COVER
- 2- FITTING TO CONNECT TO VAC. HOSE
- 3- COVER PLATE, 13 IN. DIA X 1/4 IN
- 4- DETONATOR, RP-1
- 5- O-RING GROOVE
- 6- P-80 PLANE WAVE LENS
- 7- LUCITE TUBE, 11 INCH ID X 1/2 INCH WALL
- 8- COMP. B. PAD, 8 INCH X 7 INCH X 1 INCH
- 9- STEEL BUFFER PLATE
- 10- ALUMINUM DRIVEN PLATE
- 11- ALUMINUM DRIVEN PLATE
- 12- FIRST PMMA BUFFER PLATE
- 13- GAUGES UNDER TEST
- 14- ALUMINUM BUFFER PLATE
- 15- SECOND PMMA BUFFER PLATE
- 16- UPPER SUPPORT BLOCKS, BEA NOT BOUNDED
- 17- C-7 EPOXY GAUGE BACKING MAT'L
- 18- LOWER SUPPORT BLOCKS, BEA BOUNDED
- 19- 1/4-20 BOLT, BEA
- 20- VACUUM TIGHT EPOXY FILLET AROUND SIGNAL LEADS
- 21- O-RING GROOVE
- 22- PZ T.O.A. PIN, 4 EA. EQ. SP. ON A 6.0 IN BOLT CIRCLE

Figure 13 Explosive plane wave lens.

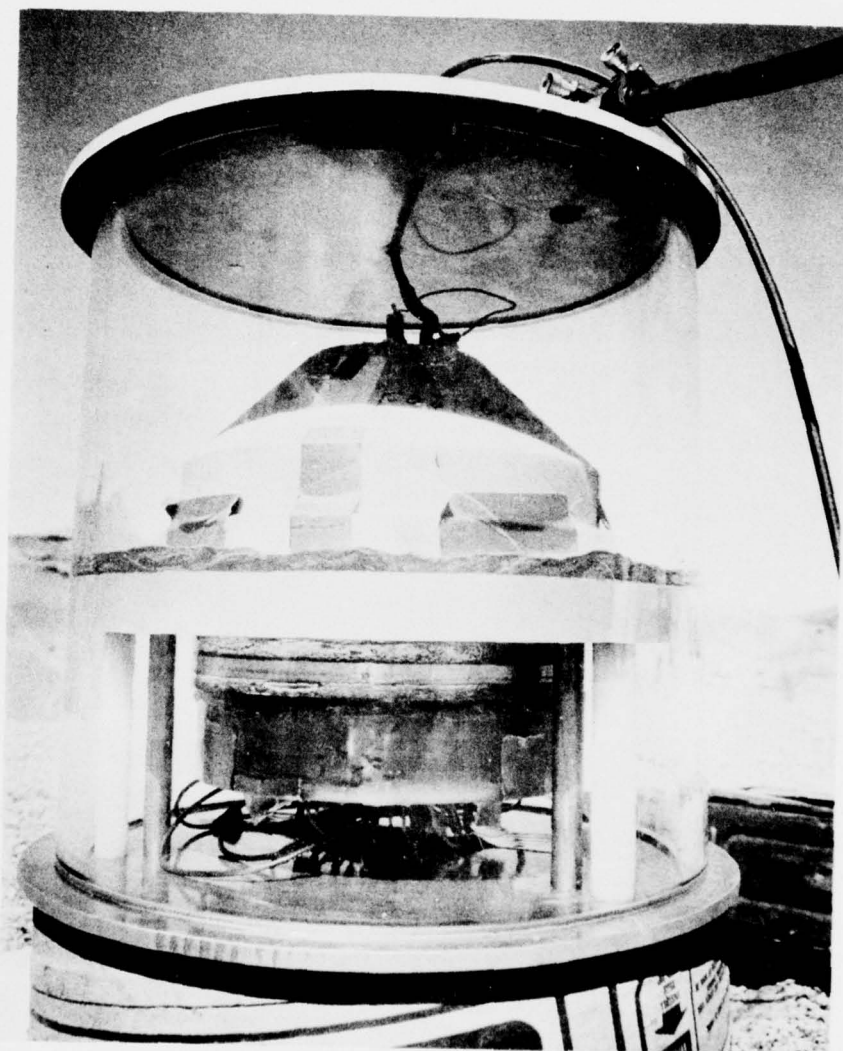
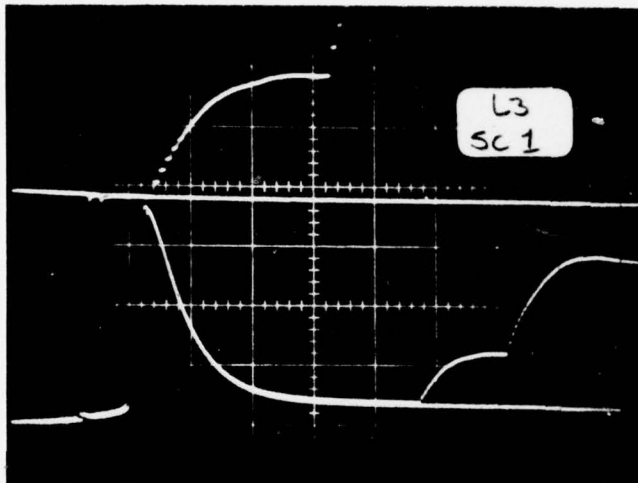


Figure 14 Plane wave lens experimental setup,
ready for firing.

Three shots were fired. On the first shot, in which manganin, carbon, cerium, and thallium/indium gauges were used, early time failure of the cables occurred, resulting in loss of all data. On subsequent shots where bismuth, bismuth/lead, ammonium iodide, and thiourea gauges were included, additional shielding and minor rerouting of the cables successfully eliminated this problem. Excellent quality manganin and carbon gauge records were obtained on the second and third shots. The manganin gauge records are shown in Figures 15 and 16. Unfortunately the records obtained for the materials under evaluation indicated that in each instance the phase change gauge circuits opened promptly upon the arrival of the initial shock wave.

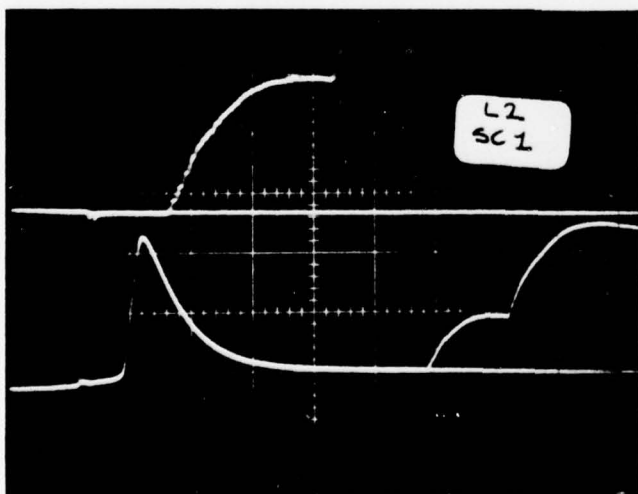
Comparing the measured manganin gauge records with the pre-test computation (Figure 17), the observed peak stress was considerably higher than predicted. Upon re-examination of the calculational configuration versus the actual experimental configuration, it was discovered that in the calculations, the 1-inch-thick pad of Comp-B was replaced with a theoretical 1-inch-thick pad of Baratol, the primary constituent of the plane wave lens. The calculation was repeated, taking into account the presence of the 1-inch-thick pad of Comp-B and the results much more closely match the experimental results. Figure 18 is a plot of the experimental and calculational pressure versus time histories.

Although the peak pressures obtained in the calculations are much closer to the experimentally derived peak pressures, there is a significant difference. Additionally, the waveform of the calculations is much different from experiment, beyond the initial pressure rise to 25 kilobars. Since it was this initial portion of the waveform that was of interest, the calculation with the Comp-B included more closely represents reality.



Upper beam: 0.5 μ sec/div
2.0 V/div

Lower beam: 1.0 μ sec/div
5.0 V/div



Upper beam: 0.5 μ sec/div
2.0 V/div

Lower beam: 1.0 μ sec/div
5.0 V/div

Figure 15 Manganin gauge records from Shots ISGC-L2 and ISGC-L3.

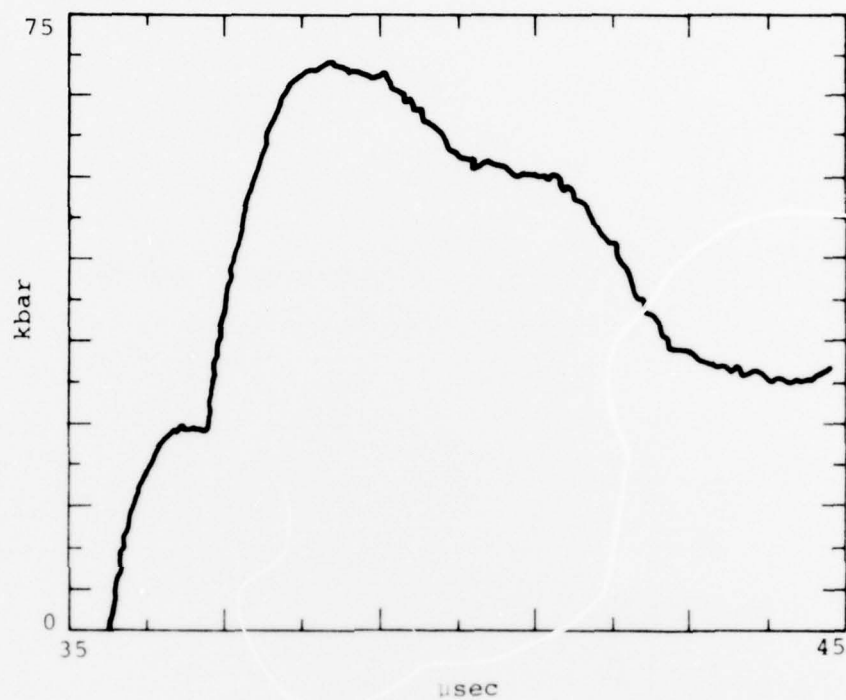


Figure 16 Manganin gauge record from shot ISGC-L2.

PISCES LCL DATE = 14 JUN 76
P-80 LENS WITH ALUMINUM FLYER PLATE INTO BUFFERS DOUBLE ZONES

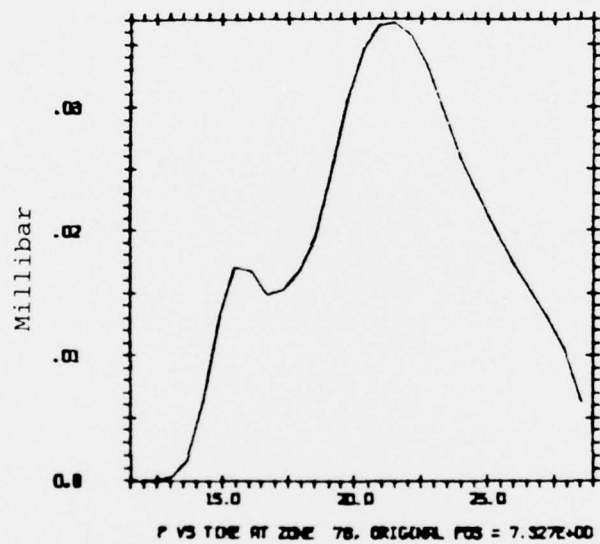


Figure 17 Computational results for experiments; pressure shown is taken at the gauge plane.

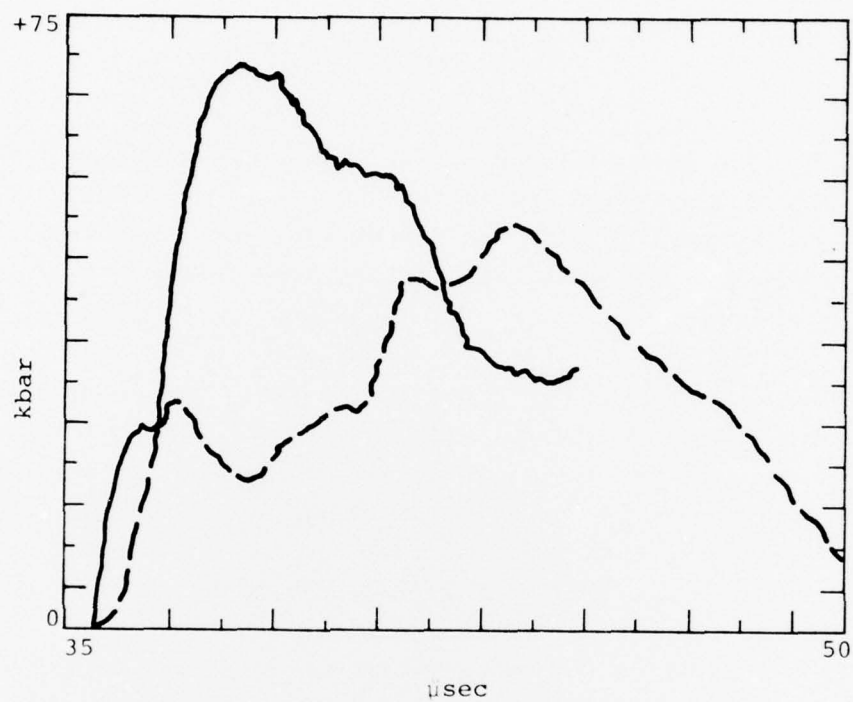


Figure 18 Experimental results plotted against calculational results including Comp-B Pad (solid line represents experimental results).

SECTION 6

GAUGE FABRICATION EFFORTS

After the failures experienced during the plane wave lens shots, the gauge design and fabrication procedures were carefully reviewed. Comparison with the gauges that were successful in the gas-gun experiments identified critical construction areas which could have led to the failure of the gauges.

The most probable cause for the failures was identified as the use of C-7 epoxy for the backing material behind the gauge element, in contrast to the fused silica utilized as a backing in most of the gas-gun shots. Specifically, the difficulty occurred in the vapor deposited conductor used to make an electrical connection between the active element of the gauge and the gauge leads taking the signal out of the epoxy backing. It is likely that upon arrival of the shock front, shear forces at the impedance discontinuity between the end of the copper leads and the C-7 epoxy ruptured the vapor plated connection.

To overcome this difficulty, the final portion of the program consisted of designing and fabricating a set of gauges that could be used in future tests. The design of the gauges is shown in Figure 19. To prevent the development of shear failure in early times after the arrival of the shock front, the gauge active element will be sandwiched between two substrates of sapphire. These sapphire substrates are 0.003 inch thick, which will give the gauges a rapid equilibration time with the surrounding media. Additionally, the sapphire is sufficiently rigid to impart significant mechanical strength to the gauge package before it is emplaced in a test configuration.

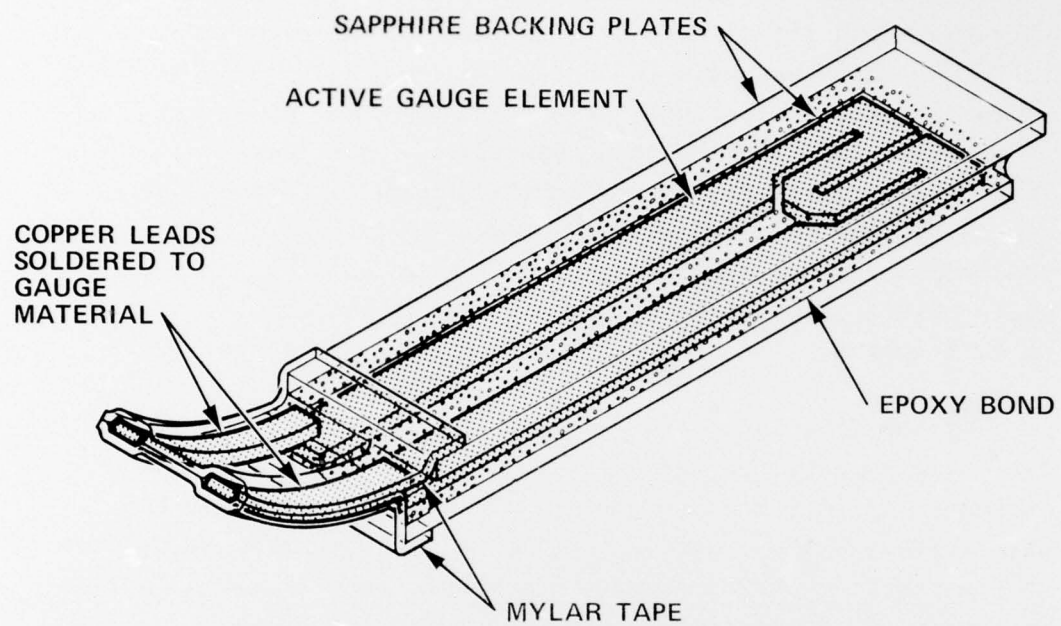


Figure 19 Phase-change gauge configuration.

An unforeseen characteristic of the conductive materials selected as candidates for the phase transition gauges is the very high conductivity of the elements. As an example, the thallium/indium gauges used in the gas-gun and plane wave lens tests exhibited resistances of about 0.25 ohm. It is thus necessary to fabricate a gauge having multiple legs in grid form so that the resistance is sufficiently high for a reasonable signal to be produced during the phase transition. To accomplish this multi-legged gauge pattern, it is necessary to utilize a photo mask process similar to that used in fabricating printed circuit boards.

Of the four materials selected for use in the gauges, only two are etched by the standard ferric chloride circuit board etchant. These two materials are the bismuth metal and the bismuth/lead alloy. Neither cerium nor thallium/indium responds to the ferric chloride etchant. Both of these latter materials do respond to concentrated nitric acid and are quite soluble in this acid, as is the photo-resist used to protect the desired gauge configuration during the etching process.

Fabrication of the ferric chloride resistant material into grids is accomplished through the use of a two step process. Both cerium and thallium/indium are soluble in concentrated nitric acid; however, copper is not. Use of this selective solubility allows a copper sheet to be bonded to the surface of the material to be etched, and a photo-resist gauge pattern applied. The two layer package is then placed in a ferric chloride etchant bath, and the unprotected copper etched away. The package is then switched to a nitric acid bath, and the gauge material now unprotected by the copper layer is etched away. The last remnants of the photo-resist are then removed from the surface of the remaining copper, and the package is

placed in the ferric chloride bath to remove the copper from the surface of the gauge element. The result is a grid element of a material that is resistant to etching by ferric chloride. Figure 20 shows the design of the photo mask for making the active gauge elements.

Due to the difficulties encountered in fabrication attempts with the cerium metal, which is quite reactive with both air and epoxies, this material has been dropped from consideration. Also since the nonconductor candidate material requires the use of a capacitance gauge, which is rather difficult to utilize, for confirmation of the evidence gained in the gas-gun shots on the validity of the phase transition technique for verifying gauge performance, these nonconducting materials have been dropped from consideration at this time.

A total of two gauges have been fabricated during this last portion of the program. The materials utilized are bismuth and bismuth/lead alloy. The intent in this effort is for future contracts to allow these gauges to verify the concept of gauge calibration. Figure 21 shows one of the gauges in its fully constructed form.

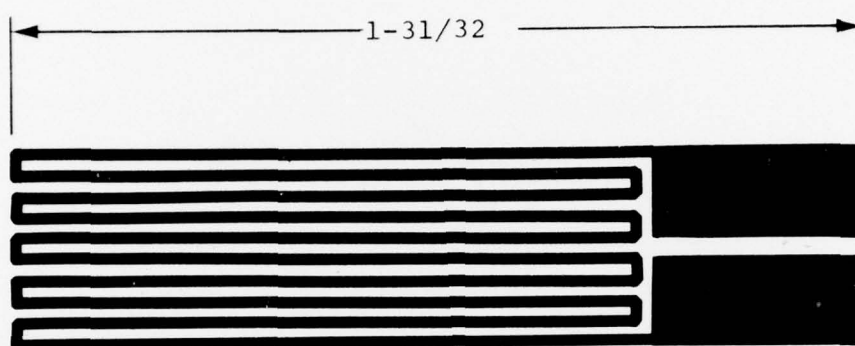


Figure 20 Photo mask pattern for phase-transition gauge active element.

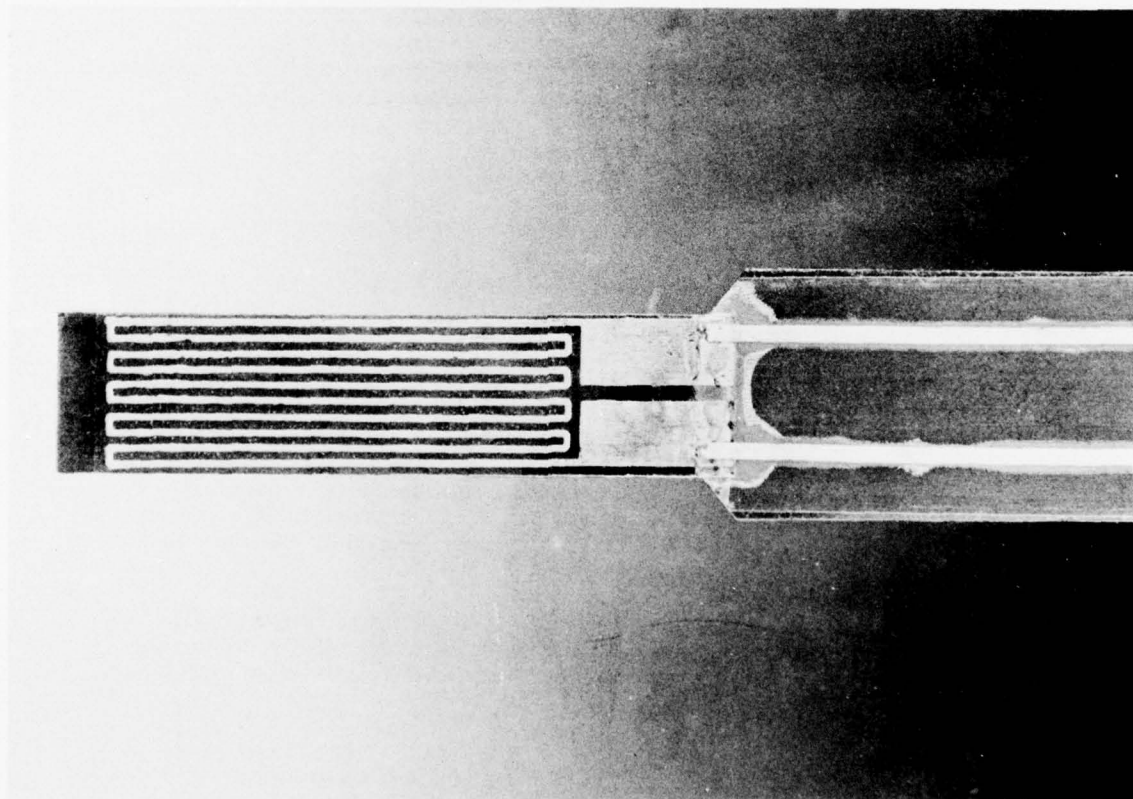


Figure 21 Bismuth gauge on sapphire substrate.

SECTION 7

CONCLUSIONS

The program conducted to examine the feasibility of providing in situ verification of stress gauge operation has led to a greater understanding of the capability of various materials and methods for providing such characteristics. Specifically:

- A variety of materials are available that undergo a phase transition at a range of pressures consistent with stress measurements conducted on large high-explosive and nuclear tests, i.e., $\frac{1}{2}$ kbar to 25 kbars.
- The most usable of these materials exhibits a change in the resistivity of the material during the phase transition.
- Other materials are available that are nonconductors; however, the use of these materials requires implementation of a capacitance gauge.
- Materials tested under the program that exhibited a measurable change in resistivity included bismuth metal, bismuth/lead alloy, thallium/indium alloy, and cerium metal.
- Results obtained from capacitance gauge tests were inadequate to determine whether a phase transition and accompanying change in dielectric constant had taken place under dynamic load conditions.
- Construction of the gauge package to ensure continued continuity during the test period is absolutely necessary to allow adequate determination of the transition pressure and required time period.
- It is necessary to test the phase transition gauges in divergent stress wave geometry as well as uniaxial stress wave geometry before complete evaluation of the concept can be made.

REFERENCES

1. D. D. Keough, C. W. Smith and M. Cowperthwaite, Constitutive Relations from In Situ Lagrangian Measurements of Stress and Particle Velocity, Interim Report, Contract DASA 01-70-C-0098, January 1971.
2. C. Godfrey, Strength of In-Situ Rock, PIIR-5-73, Physics International Company, San Leandro, California, February 1973.
3. C. A. Swenson, Solid State Physics, Vol. 17, Seitz and Turnbull, Eds., Academic Press, New York and London, (1960).
4. W. Paul, "Electrical Properties of Metals and Semiconductors," High Pressure Physics and Chemistry, Vol. 1, R. S. Bradley, Ed., Academic Press, N.Y., 1963.
5. D. G. Doran, R. K. Linde, Solid State Physics, Vol. 19, Seitz and Turnbull, Eds., Academic Press, N.Y., 1966.
6. D. L. Styris, and G. E. Duvall, High Temperatures-High Pressures, Vol. 2, pp. 477-499, 1970.
7. W. J. Murri, D. R. Curran, C. F. Peterson, and R. C. Crewdson, Response of Solids to Shock Waves, Poulter Lab Tech Report 001-71, Stanford Research Institute, Menlo Park, Ca.
8. O. E. Jones, and R. A. Graham, Shear Strength Effects on Phase Transition "Pressures" Determined from Shock-Compression Experiments. Paper presented at Symposium on Accurate Characterization of the High Pressure Environment, National Bureau of Standards, Gaithersburg, Md., Oct. 14-18, 1968.
9. S. N. Vaidya, and G. C. Kennedy, Compressibility of 18 Metals to 45 kbar, J. Phys. Chem. Solids, 31, 2329-2345 (1970).
10. R. Grover, Comments on the Comparison of Dynamic and State Compression Data, J. Phys. Chem. Solids, 32, 2347-2351 (1970).
11. D. D. Keough, and J. Y. Wong, J. Appl Phys, 41, 8, 3509-3515 (1970).
12. Private Communication of D. Keough, concerning unreported work by W. Murri, Stanford Research Institute.

13. P. W. Bridgman, Proc. Am. Acad. Arts Sci., 76, 55-70 (1948).
14. P. W. Bridgman, Proc. Nat'l Acad. Sci. U.S., 21, 109-113 (1935).
15. P. W. Bridgman, Proc. Am. Acad. Arts Sci., 76, 71-87 (1948).
16. P. W. Bridgman, Proc. Am. Acad. Arts Sci., 76, 9-24 (1945).
17. P. W. Bridgman, Proc. Am. Acad. Arts Sci., 76, 1-7 (1945).
18. P. W. Bridgman, Proc. Am. Acad. Arts Sci., 74, 21-51 (1940).
19. P. W. Bridgman, Phys. Rev., 60, 351-354 (1941).
20. P. W. Bridgman, Proc. Am. Acad. Arts Sci., 84, 43-109 (1955).
21. P. W. Bridgman, Proc. Am. Acad. Arts Sci., 84, 1-42 (1955).
22. P. W. Bridgman, Proc. Am. Acad. Arts Sci., 81, 167-251 (1952).

DISTRIBUTION LIST

DEPARTMENT OF DEFENSE

Director
Defense Advanced Research Proj. Agency
ATTN: Technical Library
ATTN: NMRO
ATTN: PMO
ATTN: STO

Defense Documentation Center
Cameron Station
12 cy ATTN: TC

Director
Defense Nuclear Agency
2 cy ATTN: SPSS
ATTN: TISL, Archives
3 cy ATTN: TITL, Tech. Library
ATTN: DDST

Commander
Field Command
Defense Nuclear Agency
ATTN: FCTMOF
ATTN: FCT
ATTN: FCPR

Chief
Livermore Division, Field Command, DNA
Lawrence Livermore Laboratory
ATTN: FCPRL

Dir. of Defense Research & Engineering
Dept. of Defense
ATTN: S&SS (OS)

DEPARTMENT OF THE ARMY

Dep. Chief of Staff for Research Dev. & Acq.
Department of the Army
ATTN: Technical Library

Commander
Harry Diamond Laboratories
ATTN: DRXDO-NP
ATTN: DRXDO-TI, Tech. Lib.

Director
US Army Ballistic Research Labs.
ATTN: Tech. Lib., Edward Baicy
ATTN: DRDAR-BLE, J. H. Keefer/DRXBR-X,
Julius J. Meszaros

Director
US Army Engr. Waterways Exper. Sta.
ATTN: Leo Ingram/J. K. Ingram/William Flathau
ATTN: Technical Library
ATTN: F. Hanes

Commander
US Army Materiel Dev. & Readiness Command
ATTN: Technical Library

DEPARTMENT OF THE NAVY

Chief of Naval Research
Navy Department
ATTN: Technical Library

Officer in Charge
Civil Engineering Laboratory
Naval Construction Battalion Center
ATTN: Technical Library
ATTN: R. J. Odello

Commander
David W. Taylor Naval Ship R & D Center
ATTN: Code L42-3, Library

Commander
Naval Facilities Engineering Command
Headquarters
ATTN: Technical Library

Commander
Naval Ship Engineering Center
Department of the Navy
ATTN: Technical Library

Commander
Naval Ship Research & Development Center
Underwater Explosive Research Division
ATTN: Technical Library

Commander
Naval Surface Weapons Center
ATTN: Code WA501, Navy Nuc. Prgms. Off.

DEPARTMENT OF THE AIR FORCE

AF Geophysics Laboratory, AFSC
ATTN: SUOL, Research Lib.

AF Institute of Technology, AU
ATTN: Library AFIT, Bldg. 640, Area B

AF Weapons Laboratory, AFSC
ATTN: DEX
ATTN: DES-S
ATTN: SUL

Hq. USAF/IN
ATTN: INATA

ENERGY RESEARCH & DEVELOPMENT ADMINISTRATION

University of California
Lawrence Livermore Laboratory
ATTN: Tech. Info. Dept. L-3

Sandia Laboratories
Livermore Laboratory
ATTN: Doc. Control for Tech. Library

Sandia Laboratories
ATTN: Doc. Con. for Org. 3422-1, Sandia
Rpt. Coll.
ATTN: Doc. Con. for Luke J. Vortman/A. J.
Chaban

ENERGY RESEARCH & DEVELOPMENT ADMINISTRATION

US Energy Research & Dev. Admin.
Albuquerque Operations Office
ATTN: Doc. Con. for Tech. Library

US Energy Research & Dev. Admin.
Division of Headquarters Services
Library Branch G-043
ATTN: Doc. Con. for Class Tech. Lib.

US Energy Research & Dev. Admin.
Nevada Operations Office
ATTN: Doc. Con. for Tech. Lib.

Union Carbide Corporation
Holifield National Laboratory
ATTN: Civ. Def. Res. Proj.

OTHER GOVERNMENT AGENCIES

National Bureau of Standards
ATTN: Paul S. Lederer

DEPARTMENT OF DEFENSE CONTRACTORS

Aerospace Corporation
ATTN: Prem N. Mathur
ATTN: Tech. Info. Services

Agbabian Associates
ATTN: M. Agbabian

Artec Associates, Inc.
ATTN: D. W. Baum

Civil/Nuclear Systems Corp.
ATTN: Robert Crawford

EG & G, Inc.
Albuquerque Division
ATTN: Technical Library

General Electric Company
TEMPO-Center for Advanced Studies
ATTN: DASIAC

IIT Research Institute
ATTN: Technical Library

Kaman Sciences Corporation
ATTN: Donald C. Sachs
ATTN: Library

Merritt Cases, Incorporated
ATTN: Technical Library
ATTN: J. L. Merritt

The Mitre Corporation
ATTN: Library

Nathan M. Newmark
Consulting Engineering Services
ATTN: W. Hall
ATTN: Nathan M. Newmark

DEPARTMENT OF DEFENSE CONTRACTORS (Continued)

Physics International Company
ATTN: Doc. Con. for Tech. Lib.
ATTN: Doc. Con. for Coye Vincent
ATTN: Doc. Con. for Fred M. Sauer/Charles
Godfrey
ATTN: K. Seifert
ATTN: J. Shea

R & D Associates
ATTN: J. G. Lewis/C. P. Knowles
ATTN: Technical Library

Science Applications, Inc.
ATTN: Technical Library

Southwest Research Institute
ATTN: A. B. Wenzel
ATTN: Wilfred E. Baker

Stanford Research Institute
ATTN: Burt R. Gasten/P. DeCarli
ATTN: George R. Abrahamson

Systems, Science & Software, Inc.
ATTN: Technical Library
ATTN: Donald R. Grine

TRW Systems Group
2 cy ATTN: Peter K. Dai, RI/2170
ATTN: Tech. Info. Center/S-1930

TRW Systems Group
San Bernardino Operations
ATTN: E. Y. Wong, 527/712

The Eric H. Wang
Civil Engineering Research Fac.
University Station
ATTN: Neal Baum

Weidlinger Assoc. Consulting Engineers
ATTN: Melvin L. Baron

Weidlinger Assoc. Consulting Engineers
ATTN: J. Isenberg

Electrical Systems of New Mexico
ATTN: R. A. Shunk

H-Tech. Laboratories
ATTN: Bruce Hartenbaum